Journal of Computational Physics 229 (2010) 5630–5652

Contents lists available at ScienceDirect

Journal of Computational Physics

journal homepage: www.elsevier.com/locate/jcp

Asymptotic-Preserving Particle-In-Cell method for the Vlasov–Poisson system near quasineutrality

Pierre Degond [a,b], Fabrice Deluzet [a,b], Laurent Navoret [a,b], An-Bang Sun [a,b,c], Marie-Hélène Vignal [a,b,*]

[a] Université de Toulouse, UPS, INSA, UT1, UTM, Institut de Mathématiques de Toulouse, F-31062 Toulouse, France
[b] CNRS, Institut de Mathmatiques de Toulouse, UMR 5219, F-31062 Toulouse, France
[c] The College of Astronautics, Northwestern Polytechnical University, No. 127 Youyi Xilu, Xi'an, China

ARTICLE INFO

Article history:
Received 3 February 2009
Received in revised form 5 November 2009
Accepted 2 April 2010
Available online 13 April 2010

Keywords:
Vlasov–Poisson
Quasineutral limit
Asymptotic-Preserving scheme
Plasma
Debye length

ABSTRACT

This paper deals with the numerical resolution of the Vlasov–Poisson system in a nearly quasineutral regime by Particle-In-Cell (PIC) methods. In this regime, Classical PIC methods are subject to stability constraints on the time and space steps related to the small Debye length and large plasma frequency. Here, we propose an "Asymptotic-Preserving" PIC scheme which is not subjected to these limitations. Additionally, when the plasma period and Debye length are small compared to the time and space steps, this method provides a consistent PIC discretization of the quasineutral Vlasov equation. We perform several one-dimensional numerical experiments which provide a solid validation of the method and its underlying concepts, and compare the method with Classical PIC and Direct-Implicit methods.

1. Introduction

The impact of plasmas and more generally, charged-particle fluids on the human environment is constantly increasing, due to their importance in such domains as industrial processes, energy, lighting, air or water cleaning, etc. Because of the large variety of physical situations and the complex multiscale character of most plasma phenomena, the numerical simulation of plasmas still represents an important challenge for the scientific community. Roughly speaking, according to the physical context, two large classes of mathematical models can be used: fluid models and kinetic ones. This paper is concerned with collisionless plasmas for which a kinetic description is required.

The basic kinetic model for plasma simulations is the Vlasov equation, coupled with the electromagnetic field equations. The Vlasov equation is posed on a 6-dimensional phase-space (3 space dimensions and 3 velocity dimensions) plus time. For this reason, particle methods have been preferred to grid-based (Eulerian) methods, as they allow a coarse, yet sufficiently precise, description of the phase-space. In Particle-In-Cell methods, the coupling between the particles and the field is implemented through the introduction of a space grid. Charge and current densities are assigned from the particles to the grid. Then, the fields are computed using finite difference methods on the grid and then, interpolated back to the positions of the particles. We refer to the two celebrated books [3,27] for an overview of these methods. Recently, grid-based Eulerian simulations have received a great deal attention [1,6,16–18,38,40] but particle methods are still the number-one method

* Corresponding author at: Université de Toulouse, UPS, INSA, UT1, UTM, Institut de Mathématiques de Toulouse, F-31062 Toulouse, France. Tel.: +33 5 61 55 69 22; fax: +33 5 61 55 83 85.
E-mail addresses: pierre.degond@math.univ-toulouse.fr (P. Degond), fabrice.deluzet@math.univ-toulouse.fr (F. Deluzet), laurent.navoret@math.univ-toulouse.fr (L. Navoret), an-bang.sun@math.univ-toulouse.fr, absun1984@hotmail.com (A.-B. Sun), mhvignal@math.univ-toulouse.fr (M.-H. Vignal).

0021-9991/$ - see front matter © 2010 Elsevier Inc. All rights reserved.
doi:10.1016/j.jcp.2010.04.001

used for the numerical simulation of plasma kinetic models. The convergence of PIC methods has been mathematically investigated in [9,19].

One of the very basic but very important problem in plasma simulations is the handling of quasineutrality. Indeed, the electrostatic force tends to restore the local charge neutrality of the plasma. The Debye length and plasma periods [7,30] set the typical space and time scales at which this restoring force acts. The Debye length measures the typical scale of charge unbalances in the plasma whereas the electron plasma period characterizes the oscillation period of the particles when a departure to quasineutrality occurs. Usually, both these space and time scales are very short compared to the typical scales of the phenomena under investigation. In such situation, the plasma is locally quasineutral. These very short time scales make numerical simulations very time consuming. Indeed, standard explicit PIC methods require a stability condition which guarantees that the space and time steps are smaller than the Debye length and electron plasma period.

Lots of efforts have been devoted to the search for implicit PIC schemes which would be free of such constraints. There are basically two classes of implicit PIC methods: the direct implicit method [8,31] and the implicit moment method [33,34]. In the direct implicit method, an implicit algorithm for the advancement of the particles is introduced. However, since a full implicit resolution of the particle positions and of the fields is virtually impossible, a two-step predictor–corrector approximation is practically implemented. In the implicit moment method, a prediction of the value of the fields at the next time-step is done through the use of the moment equations. Numerous extensions of these methods can be found in the literature, especially concerning the coupling with the Maxwell equations [4,25,32,35,36,41].

Recently, new classes of methods for singular perturbation problems have emerged. These are the so-called Asymptotic-Preserving (AP) methods. Let (S_λ) be a singularly perturbed system and (S_0) the limit system when $\lambda \to 0$. Here, we give a definition of an AP method.

Definition 1. An Asymptotic-Preserving scheme for (S_λ) in the limit $\lambda \to 0$ is a scheme which is consistent with (S_λ) when the numerical parameters (e.g. Δx, Δt) resolve the scales associated with the small parameter λ and which is consistent with (S_0) when $\lambda \to 0$ with Δt, Δx staying of order one.

The concept of AP method originates from the work of Shi Jin for multiscale kinetic equations [28]. In our case, (S_λ) is the Vlasov–Poisson system and (S_0) is the quasineutral Vlasov system.

The concept of AP method is particularly interesting when λ is not uniformly small. For instance, at a plasma edge, the parameter λ, which depends on the local value of the plasma density, can vary by several orders of magnitude from $\lambda \ll 1$ to $\lambda = O(1)$. In this case, the original problem (S_λ) must be solved in the region where $\lambda = O(1)$ and the limit problem (S_0), where $\lambda \ll 1$. With classical method, this situation requires a model coupling methodology to connect the two models. However, model coupling methods involve a certain level of arbitrariness, such as the location of the coupling interface or the expression of the coupling terms. Their implementation can also be quite complex with the need to adapt the mesh to the geometry of the interface. The AP method allows the computation of the two regions $\lambda = O(1)$ and $\lambda \ll 1$ with the same and unique method. The AP scheme automatically shifts from the (S_λ) model to the (S_0) model wherever λ becomes small, without any need to reduce the time and space steps. This results in a considerably more robust numerical code. We shall see an example of this situation with the simulation of the expansion of an ion slab at Section 4.4.

In this paper, we propose an Asymptotic-Preserving PIC method (or PICAP method) for the Vlasov–Poisson equation in the quasineutral limit. Previous works on AP methods for the quasineutral limit have been devoted to the Euler–Poisson problem [10,12,14] and to Eulerian schemes for the Vlasov–Poisson problem [2]. The quasineutral limit in plasmas has been theoretically investigated in [5,11,15,20,21,24,37].

The present work is a follow-up of a previous work [13], where a first variant of the method (the PICAP-1 method) was presented and tested on a one-species model of a perturbed Maxwellian plasma. In the present work, we introduce a new, simpler variant of this method (the PICAP-2 method) and considerably broaden the list of test problems. These are,

1. a steady-state simulation to quantify the dissipation of the scheme,
2. one and two species perturbations of a Maxwellian plasma with a particular consideration of the Landau damping test problem,
3. the Bump-on-Tail instability,
4. the expansion of an ion slab, following [22,23].

We will also compare our method to various variants of the Direct-Implicit method.

The method relies on the remark that the equation allowing the computation of the potential in the quasineutral Vlasov problem is very different from the Poisson equation. Indeed, the former is an elliptic equation found from the divergence free condition on the current, a consequence of the quasineutrality. To build an AP scheme, it is necessary to find a unified framework for both the Poisson equation and the quasineutral potential equation. This is done by reformulating the Poisson equation into a strictly equivalent equation which explicitly contains the quasineutral potential equation as a particular case when $\lambda = 0$. This equation is differential in both time and space, and specifically second order in time. An implicit discretization of this equation is combined with a semi-implicit discretization of the particle trajectories and yields an Asymptotic-Preserving scheme for the Vlasov–Poisson problem in the quasineutral limit. Since the reformulation of the Poisson equation leads to a fully equivalent problem, there is no other approximation involved in our method than purely numerical ones (i.e.

associated to the time and space discretization). To our knowledge, previous implicit methods such as the direct implicit or the moment implicit ones (see references above) have not been analyzed in view of this Asymptotic Preservation property, and we will show that they are not consistent with the quasineutral limit problem when $\lambda \to 0$.

This paper is organized as follows. In Section 2, we present the two-fluid Vlasov–Poisson system model and its quasineutral limit and we derive the reformulated Poisson equation. From this reformulation, in Section 3, we build up the Asymptotic-Preserving Particle-In-Cell (PICAP) method. Section 4 is devoted to the discussion of the numerical results: comparisons between the classical and Asymptotic-Preserving schemes are provided in a one-dimensional geometry. We consider the various test problems as listed above. The results confirm that the AP strategy remains stable and provides the expected results even if the time and space discretizations do not resolve the Debye length and plasma periods. This shows that the method can powerfully deal with stiff problems when the stiffness results from the quasineutrality constraint. By contrast, the Direct-Implicit method show lower accuracy in stiff problems such as the expansion of an ion slab problem.

2. The Vlasov–Poisson system and its quasineutral limit

In this section, we present the two-fluid Vlasov–Poisson system and its quasineutral limit.

2.1. The Vlasov–Poisson system

We are interested in the kinetic description of a two-fluid plasma constituted of electrons and one ion species. Then, ions and electrons are described by their distribution function respectively denoted by $f_i(x, v, t)$ and $f_e(x, v, t)$, where the position and velocity variables x and v are such that $(x, v) \in \Omega \times \mathbb{R}^d$, with $\Omega \subset \mathbb{R}^d$ and $d = 1, 2$, or 3 and $t \geqslant 0$ is the time. The two-fluid Vlasov–Poisson system is written:

$$\partial_t f_i + v \cdot \nabla_x f_i - \frac{e}{m_i} \nabla_x \phi \cdot \nabla_v f_i = 0, \tag{2.1}$$

$$\partial_t f_e + v \cdot \nabla_x f_e + \frac{e}{m_e} \nabla_x \phi \cdot \nabla_v f_e = 0, \tag{2.2}$$

where we denote by $e > 0$ the positive elementary charge, by $m_{i,e}$ the ion and electron masses and by ϕ the electric potential. ϕ is given by the Poisson equation:

$$-\Delta \phi = \frac{e}{\varepsilon_0}(n_i - n_e), \tag{2.3}$$

where ε_0 is the vacuum permittivity, and $n_{i,e}$ are the ion and electron densities, given by

$$n_i(x,t) = \int_{\mathbb{R}^d} f_i(x, v, t)\, dv, \quad n_e(x,t) = \int_{\mathbb{R}^d} f_e(x, v, t)\, dv.$$

The two important physical scales for this model are the Debye length λ_D and the electron plasma frequency ω_p given by:

$$\lambda_D = \left(\frac{\varepsilon_0 k_B T_0}{e^2 n_0}\right)^{1/2}, \quad \omega_p = \left(\frac{n_0 e^2}{\varepsilon_0 m_e}\right)^{1/2},$$

where k_B is the Boltzmann constant, n_0 is the plasma density scale ($n_0 \backsim n_i \backsim n_e$), T_0 is the plasma temperature scale. We note that an ion plasma frequency can be defined (replacing m_e by m_i). However, this parameter is smaller than ω_p because of the large ion to electron mass ratio. The electron plasma period is defined by $\tau_p = 1/\omega_p$.

The situation where both the Debye length and electron plasma period are very small compared with the typical macroscopic length and time scales is called the quasineutral regime because the local electric charge is very small (of order $k^2\lambda_D^2$ where k is the local inverse gradient length of the electric potential). Simultaneously, the electron plasma period becomes very small as well, so that when local charge unbalances occur (at the scale of the Debye length), very high plasma frequency oscillations are triggered.

In order to study the quasineutral model, we introduce the following scaling of the Vlasov–Poisson problem. The scaled variables are given by

$$\bar{x} = \frac{x}{x_0}, \quad \bar{v} = \frac{v}{v_0}, \quad \bar{t} = \frac{v_0}{x_0} t, \quad \bar{n}_{i,e} = \frac{n_{i,e}}{n_0}, \quad \bar{f}_{i,e} = \frac{v_0}{n_0} f_{i,e}, \quad \bar{\phi} = \frac{e\phi}{k_B T_0}, \tag{2.4}$$

where $x_0 > 0$ is the typical length of the problem, and $v_0 \in \mathbb{R}$ is the thermal ion velocity scale given by $v_0 = (k_B T_0/m_i)^{1/2}$. Inserting this scaling into Eqs. (2.1)–(2.3) and omitting the bars, we get the following scaled two-fluid Vlasov–Poisson model

$$\partial_t f_i + v \cdot \nabla_x f_i - \nabla_x \phi \cdot \nabla_v f_i = 0, \tag{2.5}$$

$$\partial_t f_e + v \cdot \nabla_x f_e + \frac{1}{\varepsilon} \nabla_x \phi \cdot \nabla_v f_e = 0, \tag{2.6}$$

$$-\lambda^2 \Delta \phi = (n_i - n_e), \quad n_{i,e} = \int f_{i,e}\, dv. \tag{2.7}$$

where $\lambda = \lambda_D/L$ is the scaled Debye length and $\varepsilon = m_e/m_i$ is the electron to ion mass ratio. Note that the scaled plasma frequency is given by $\omega = \omega_p x_0/v_0 = 1/(\sqrt{\varepsilon}\lambda)$. In the following, we investigate the limit $\lambda \to 0$ which leads to the quasineutral limit.

In the forthcoming test cases, we will also be interested in the one-species case, considering only electrons while ions are supposed static (due to their very large mass). The scaled one-species Vlasov–Poisson problem is written:

$$\partial_t f + v \cdot \nabla_x f + \nabla_x \phi \cdot \nabla_v f = 0, \tag{2.8}$$

$$-\lambda^2 \Delta \phi = (n_0 - n), \quad n = \int f \, dv, \tag{2.9}$$

where n_0 is supposed to be a uniform ion background density.

2.2. Reformulation of the Poisson equation

The quasineutral limit consists in letting $\lambda \to 0$ in the scaled Vlasov–Poisson system (2.5)–(2.7). Obviously, when $\lambda = 0$, we lose the possibility of using the Poisson equation (2.7) to compute the potential ϕ since (2.7) reduces to the quasineutrality constraint $n_i = n_e$. For this reason, we introduce a reformulation of the problem which provides a more convenient approach to the quasineutral limit.

To this aim, we take the velocity moments of Eqs. (2.5) and (2.6) and obtain the mass and momentum conservation equations:

$$\partial_t n_i + \nabla \cdot (nu)_i = 0, \tag{2.10}$$

$$\partial_t (nu)_i + \nabla \cdot S_i = -n_i \nabla \phi, \tag{2.11}$$

$$\partial_t n_e + \nabla \cdot (nu)_e = 0, \tag{2.12}$$

$$\partial_t (nu)_e + \nabla \cdot S_e = \frac{n_e}{\varepsilon} \nabla \phi, \tag{2.13}$$

where $(nu)_{i,e}$, the ion and electron momenta and $S_{i,e}$, the (specific) momentum fluxes are given by

$$(nu)_{i,e} = \int_{\mathbb{R}^d} f_{i,e}(x, v, t) v \, dv, \quad S_{i,e} = \int_{\mathbb{R}^d} f_{i,e}(x, v, t) v \otimes v \, dv,$$

and the symbol $\otimes$ denotes the tensor product. Taking the differences of (2.10) and (2.12) on the one hand, and of (2.11) and (2.13) on the other hand, we get the continuity and current equations respectively:

$$\partial_t (n_i - n_e) + \nabla \cdot ((nu)_i - (nu)_e) = 0. \tag{2.14}$$

$$\partial_t ((nu)_i - (nu)_e) + \nabla \cdot (S_i - S_e) = -\left(n_i + \frac{n_e}{\varepsilon}\right) \nabla \phi. \tag{2.15}$$

Taking the time derivative again of (2.14) and the divergence of (2.15) and subtracting the resulting two equations leads to:

$$\partial_t^2 (n_i - n_e) - \nabla^2 : (S_i - S_e) = \nabla \cdot \left(\left(n_i + \frac{n_e}{\varepsilon}\right) \nabla \phi \right), \tag{2.16}$$

where ∇^2 denotes the tensor of second order derivatives and ":" the contracted product of two tensors. After substitution of the Poisson equation (2.7), this equation yields:

$$-\lambda^2 \partial_t^2 \Delta \phi - \nabla^2 : (S_i - S_e) = \nabla \cdot \left(\left(n_i + \frac{n_e}{\varepsilon}\right) \nabla \phi \right). \tag{2.17}$$

Collecting ϕ into the left-hand side, we find the so-called reformulated Poisson equation:

$$-\nabla \cdot \left(\left(n_i + \frac{n_e}{\varepsilon} + \lambda^2 \partial_t^2\right) \nabla \phi \right) = \nabla^2 : (S_i - S_e). \tag{2.18}$$

These computations show that, if the triple (f_e, f_i, ϕ) solves the Vlasov–Poisson problem (2.5)–(2.7), it solves the "reformulated Vlasov–Poisson problem" consisting of the Vlasov equations (2.5), (2.6) and the reformulated Poisson equation (2.18). Conversely, if the triple (f_e, f_i, ϕ) solves the reformulated Vlasov–Poisson problem, we find, going backwards in the previous computations, that ϕ satisfies:

$$\partial_t^2 (-\lambda^2 \Delta \phi - (n_i - n_e)) = 0.$$

Therefore, if the initial data $\phi_0 := \phi|_{t=0}$ and $\phi_0' := (\partial_t \phi)|_{t=0}$ satisfy the two Poisson equations at the initial time:

$$-\lambda^2 \Delta \phi_0 = (n_i - n_e)_0, \tag{2.19}$$

$$-\lambda^2 \Delta \phi_0' = (n_i - n_e)_0' = -\nabla \cdot ((nu)_i - (nu)_e)_0, \tag{2.20}$$

(with obvious notations), then the Poisson equation (2.7) is satisfied at all times. Since Eq. (2.18) is second order in time, it requires the knowledge of the two initial conditions ϕ_0 and ϕ_0'. Therefore, it is always possible to impose (2.19) and (2.20). A linearized stability analysis would in principle be needed to guarantee that, when (2.19) and (2.20) are not satisfied (for instance, in the discrete case, because of numerical errors), unstable linear modes are not going to be excited. However, linearized stability analysis depends on the state about which the problem is linearized and can only offer definite answers in model cases. The numerical experiments so far have not shown any instability problem of this kind (see Section 4).

We can summarize this discussion by saying that the Vlasov–Poisson system (2.5)–(2.7) is *equivalent* to the following *"reformulated Vlasov–Poisson system"*:

$$\partial_t f_i + v \cdot \nabla_x f_i - \nabla_x \phi \cdot \nabla_v f_i = 0, \tag{2.21}$$

$$\partial_t f_e + v \cdot \nabla_x f_e + \frac{1}{\varepsilon} \nabla_x \phi \cdot \nabla_v f_e = 0, \tag{2.22}$$

$$-\nabla \cdot \left(\left(n_i + \frac{n_e}{\varepsilon} + \lambda^2 \partial_t^2 \right) \nabla \phi \right) = \nabla^2 : (S_i - S_e), \tag{2.23}$$

with ϕ satisfying the initial conditions (2.19) and (2.20).

The reformulated Poisson equation has been previously proposed in the framework of fluid models in [10,12,14], and in [2,13] for plasma kinetic models.

2.3. The quasineutral limit

The quasineutral limit of the Vlasov–Poisson system has been investigated theoretically in [5,20,21] and extensively used in physical studies. It is almost impossible to cite all the relevant physical literature. We just mention [26,29,39] as examples.

The reformulation (2.21)–(2.23) allows to investigate the quasineutral limit $\lambda \to 0$ in a straightforward way. Indeed, letting $\lambda \to 0$ in (2.23), (2.19), (2.20) directly provides the following equation for the quasineutral potential ϕ:

$$-\nabla \cdot \left(\left(n_i + \frac{n_e}{\varepsilon} \right) \nabla \phi \right) = \nabla^2 : (S_i - S_e), \tag{2.24}$$

together with the two constraints

$$(n_i - n_e)_0 = 0, \tag{2.25}$$

$$(n_i - n_e)_0' = -\nabla \cdot ((nu)_i - (nu)_e)_0 = 0, \tag{2.26}$$

From these equations and with the aid of (2.16), we immediately deduce that $n_i = n_e$ at all times, which shows that quasineutrality holds.

Therefore, the limit $\lambda \to 0$ of the Vlasov–Poisson system (2.5)–(2.7), or equivalently, of its reformulation (2.21)–(2.23) leads to the following *quasi-neutral* Vlasov system:

$$\partial_t f_i + v \cdot \nabla_x f_i - \nabla_x \phi \cdot \nabla_v f_i = 0, \tag{2.27}$$

$$\partial_t f_e + v \cdot \nabla_x f_e + \frac{1}{\varepsilon} \nabla_x \phi \cdot \nabla_v f_e = 0, \tag{2.28}$$

$$-\nabla \cdot \left(\left(n_i + \frac{n_e}{\varepsilon} \right) \nabla \phi \right) = \nabla^2 : (S_i - S_e), \tag{2.29}$$

together with the initial conditions satisfying (2.25) and (2.26).

We see that, although the original and reformulated Vlasov–Poisson systems are equivalent, they are not equally well-suited in the quasineutral limit. Indeed, the quasineutral potential equation (2.29) appears as the formal limit $\lambda \to 0$ of the reformulated Poisson equation (2.23) but not of the original Poisson equation (2.7). The asymptotics does not preserve the form of the original Poisson equation while it does preserve the form of the reformulated one. Therefore, the construction of Asymptotic-Preserving schemes must be based on the use of the reformulated Poisson equation. For this reason, our Asymptotic-Preserving PIC method relies on the numerical approximation of the reformulated Vlasov–Poisson problem (2.21)–(2.23) rather than that of the original Vlasov–Poisson problem (2.5)–(2.7). We now describe the method in detail in the next section.

3. Asymptotic-Preserving PIC method (PICAP method)

3.1. PIC methods: general methodology

Particle-in-Cell (PIC) methods are widely used in the plasma physics community. We refer to the text books [3,27] for a detailed exposition (see also the bibliography in Section 1). The particle method consists in discretizing $f_{i,e}$ into a sum of delta measures located at positions $((X_{i,e})_j(t),(V_{i,e})_j(t))$ in phase-space. This is written:

$$f_{i,e}(x,v,t) \approx (f_{i,e})_N(x,v,t) := \sum_{j=1}^{N} (\omega_{i,e})_j \delta\Big(x - (X_{i,e})_j(t)\Big)\delta\Big(v - (V_{i,e})_j(t)\Big), \tag{3.1}$$

where N is the number of particles and $(\omega_{i,e})_j$ is a weight which must be conveniently defined at initialization [3,27]. The jth particle coordinates $((X_{i,e})_j(t),(V_{i,e})_j(t))$ obey Newton's equations:

$$(\dot{X}_i)_j = (V_i)_j, \quad (\dot{V}_i)_j = -\nabla_x \phi_h((X_i)_j(t),t), \tag{3.2}$$

$$(\dot{X}_e)_j = (V_e)_j, \quad (\dot{V}_e)_j = \frac{1}{\varepsilon}\nabla_x \phi_h((X_e)_j(t),t), \tag{3.3}$$

These equations are discretized in time (see discussion below). The potential ϕ_h is a space approximation of ϕ. In the PIC method, this approximation is computed at each time-step by solving the Poisson equation (2.7) on a fixed grid of space step h (e.g. using a finite difference method). An assignment procedure allows to build grid values of the particle densities $(n_{i,e})_h$ from the knowledge of the particle locations and weights. These values serve as data for the numerical resolution of the Poisson equation. Once an approximation ϕ_h on the grid has been obtained, an interpolation procedure allows to reconstruct the values of the field $\nabla_x\phi_h(X_j,t)$ at the locations of the particles. These assignment-interpolation procedures are classical and are not modified in the present work (see again [3,27]). The only modification resulting from the replacement of the original Poisson equation (2.7) by the reformulated one (2.23) is the need to assign other quantities than the densities, namely the values of the pressure tensors $S_{i,e}$. However, the assignment procedure for these quantities is the same as for the densities and does not require a specific discussion.

The major issue in making the PIC procedure Asymptotic-Preserving, besides using the reformulated Poisson equation instead of the original one, is the time discretization. In the following subsections, we successively describe the "classical" or "standard" PIC method, the PICAP method, and for the sake of comparison, we also recall the Direct-Implicit PIC method.

3.2. Classical PIC method

The Classical PIC method uses a "leap-frog" scheme where positions are defined at integer values of the time-step $X_j^m \approx X_j(m\Delta t)$, while velocities are defined at half-integer values $V_j^{m+1/2} \approx V_j((m+1/2)\Delta t)$. In the Classical PIC method, the integration of (3.2) and (3.3) is done as follows:

$$\frac{(X_{i,e})_j^{m+1} - (X_{i,e})_j^m}{\Delta t} = (V_{i,e})_j^{m+1/2}, \tag{3.4}$$

$$\frac{(V_i)_j^{m+3/2} - (V_i)_j^{m+1/2}}{\Delta t} = -\nabla_x \phi^{m+1}((X_i)_j^{m+1}), \tag{3.5}$$

$$\frac{(V_e)_j^{m+3/2} - (V_e)_j^{m+1/2}}{\Delta t} = \frac{1}{\varepsilon}\nabla_x \phi^{m+1}((X_e)_j^{m+1}), \tag{3.6}$$

where we omit the index h for the grid-approximation of the potential for simplicity. Advancing the velocities with (3.5) and (3.6) supposes that Poisson's equation (2.7) is solved with a charge density at the right-hand side of (2.7) computed from particle positions at time t^{m+1}, which is possible since these are known from (3.4). However, it is well known and widely documented in the literature [3,27] that this method suffers from a stability constraint of the form $\Delta t, h \leqslant C\lambda$ where the constant C is of order of unity. We shall refer to this scheme as the Classical PIC scheme. There have been numerous attempts to provide more stable time-stepping strategies (see the bibliography in Section 1) which have proved to be quite efficient in practical cases. However, it is not clear if these methods are consistent with the quasineutral Vlasov model (2.27)–(2.29) in the limit $\lambda \to 0$. The PICAP methods which we are going to discuss now do have this property, as we will show below.

3.3. PICAP method

In the proposed Asymptotic-Preserving strategy, positions and velocities are both defined at integer time-steps for simplicity. The time-stepping method for the position equation is fully implicit while that of the velocity equation is semi-implicit: the electric field is taken implicitly but the particle positions explicitly. More precisely, the particle time advancement scheme is as follows:

$$\frac{(X_{i,e})_j^{m+1} - (X_{i,e})_j^m}{\Delta t} = (V_{i,e})_j^{m+1}, \tag{3.7}$$

$$\frac{(V_i)_j^{m+1} - (V_i)_j^m}{\Delta t} = -\nabla_x \phi^{m+1}((X_i)_j^m), \tag{3.8}$$

$$\frac{(V_e)_j^{m+1} - (V_e)_j^m}{\Delta t} = \frac{1}{\varepsilon}\nabla_x \phi^{m+1}((X_e)_j^m). \tag{3.9}$$

The implicit evaluation of the potential ϕ^{m+1} is obtained via an implicit time-discretization of the reformulated Poisson equation (2.23).

The starting point for our implicit time-discretization of (2.23) is the following scheme:

$$-\nabla_x\cdot\left((\Delta t)^2\left(n_i^m+\frac{n_e^m}{\varepsilon}\right)\nabla_x\phi^{m+1}+\lambda^2(\nabla_x\phi^{m+1}-2\nabla_x\phi^m+\nabla_x\phi^{m-1})\right)=(\Delta t)^2\nabla_x^2:(S_i^m-S_e^m). \tag{3.10}$$

This scheme is clearly Asymptotic-Preserving in the sense of the definition stated in Section 1. Indeed, in the limit $\lambda\to 0$, we find

$$-\nabla_x\cdot\left(\left(n_i^m+\frac{n_e^m}{\varepsilon}\right)\nabla_x\phi^{m+1}\right)=\nabla_x^2:(S_i^m-S_e^m). \tag{3.11}$$

which is a consistent discretization of the quasineutral potential equation (2.29).

However, the presence of the Laplacians of the potential at the previous time-steps ϕ^m and ϕ^{m-1} at the left-hand side of (3.10) is somehow inconvenient because it introduces extra computational cost. Therefore, it is more natural to use the Poisson equation (2.7) to replace these terms by the charge densities at the corresponding time-steps.

To this aim, two strategies have been proposed. The first method, already proposed in [13] and called "PICAP-1", consists in simply performing this replacement. It leads to:

$$-\nabla\cdot\left(\left((\Delta t)^2\left(n_i^m+\frac{n_e^m}{\varepsilon}\right)+\lambda^2\right)\nabla\phi^{m+1}\right)=(\Delta t)^2\nabla^2:(S_i^m-S_e^m)+2(n_i^m-n_e^m)-(n_i^{m-1}-n_e^{m-1}). \tag{3.12}$$

Eq. (3.12) allows to compute ϕ^{m+1} from known quantities at time t^m and t^{m-1}.

Another, original method is found by using a time-discrete version of the continuity Eq. (2.14) to replace the term $(n_i^m-n_e^m)-(n_i^{m-1}-n_e^{m-1})$ at the right-hand side of (3.12) by $-\nabla((nu)_i^m-(nu)_e^m)$. This leads to the so-called "PICAP-2" method:

$$-\nabla\cdot\left(\left((\Delta t)^2\left(n_i^m+\frac{n_e^m}{\varepsilon}\right)+\lambda^2\right)\nabla\phi^{m+1}\right)=(\Delta t)^2\nabla^2:(S_i^m-S_e^m)+(n_i^m-n_e^m)-\Delta t(\nabla((nu)_i^m-(nu)_e^m)), \tag{3.13}$$

which allows to compute ϕ^{m+1} from known quantities at time t^m alone. This equation can be viewed as a discretization of the first order differential system (2.14) and (2.15). Indeed, an implicit discretization of this system is given by:

$$\frac{(n_i^{m+1}-n_e^{m+1})-(n_i^m-n_e^m)}{\Delta t}+\nabla\cdot\left((nu)_i^{m+1}-(nu)_e^{m+1})\right)=0, \tag{3.14}$$

$$\frac{((nu)_i^{m+1}-(nu)_e^{m+1}))-((nu)_i^m-(nu)_e^m))}{\Delta t}+\nabla\cdot(S_i^m-S_e^m)=-\left(n_i^m+\frac{n_e^m}{\varepsilon}\right)\nabla\phi^{m+1}. \tag{3.15}$$

Inserting (3.15) in (3.14) leads to:

$$\frac{(n_i^{m+1}-n_e^{m+1})-(n_i^m-n_e^m)}{\Delta t}+\nabla\cdot((nu)_i^m-(nu)_e^m))-(\Delta t)\nabla^2:(S_i^m-S_e^m)-(\Delta t)\nabla\cdot\left(\left(n_i^m+\frac{n_e^m}{\varepsilon}\right)\nabla\phi^{m+1}\right)=0. \tag{3.16}$$

Then replacing $(n_i^{m+1}-n_e^{m+1})$ by $-\lambda^2\Delta\phi^{m+1}$ leads to (3.13).

The advantage of the PICAP-2 method is that it does not require an auxiliary scheme to compute the first iterate at time t^1, while PICAP-1 does. The computation of the first iterate requires the use of the Classical PIC scheme. But if λ is very small, the use of the Classical PIC scheme over a single time-step can be enough to trigger an instability of the whole method. Therefore, the use of the PICAP-2 method is preferable.

In spite of the presence of the extra terms at the right-hand sides of (3.12) and (3.13) the PICAP-1 and PICAP-2 methods are Asymptotic-Preserving. Indeed, at each time-step, both differ from the AP method (3.10) by terms which are proportional to n_i-n_e and which consequently are of order $O(\lambda^2)$. Therefore, these additional terms vanish in the limit $\lambda\to 0$ and the PICAP-1 and PICAP-2 methods are Asymptotic-Preserving as well. The numerical experiments below provide an experimental evidence of this statement.

The space-discretization of the reformulated Poisson equations (3.12) or (3.13) uses standard finite-difference methods, and is omitted.

3.4. Direct-Implicit method

Here, for the sake of completeness, we describe the Direct-Implicit method of [31,32] that we have implemented for our comparisons. To describe the Direct-Implicit method, we need to introduce $(\overline{E}_{e,i})_j^m$ the electric field applied at time t^m to the jth particle, indices 'e' or 'i' referring to electrons or ions. The method is then as follows: given the electric field $(\overline{E}_{e,i})_j^m$ at time t^m, temporary particle positions and velocities are computed with the "leap-frog" scheme,

$$(\widetilde{V}_e)_j^{m+\frac12}=(V_e)_j^{m-\frac12}-\Delta t\frac{1}{\varepsilon}((1-\beta)(\overline{E}_e)_j^m-\beta\nabla\widetilde{\phi}^{m+1}((X_e)_j^m)), \tag{3.17}$$

$$(\widetilde{V}_i)_j^{m+\frac12}=(V_i)_j^{m-\frac12}+\Delta t((1-\beta)(\overline{E}_e)_j^m-\beta\nabla\widetilde{\phi}^{m+1}((X_i)_j^m)), \tag{3.18}$$

$$(\widetilde{X}_{i,e})_j^{m+1}=(X_{i,e})_j^m+\Delta t(\widetilde{V}_{i,e})_j^{m+\frac12}, \tag{3.19}$$

Table 1
Definition of the PIC schemes.

Classical PICAP-1	Eqs. (3.4)–(3.6)	explicit
PICAP-1	Asymptotic Preserving Pic, Eqs. (3.7)–(3.9), (3.12) and $\phi^{-1} = 0$	implicit
PICAP-2	Asymptotic Preserving Pic, Eqs. (3.7)–(3.9), (3.13)	implicit
C-DI ($\beta = 1/2$)	Classical Direct-Implicit, Eqs. (3.17)–(3.21) with $\beta = 1/2$	explicit–implicit
M-DI ($\beta = 1/2$)	Modified Direct-Implicit, Eqs. (3.17)–(3.21) with $\beta = 1/2$ and $\phi^0 = 0$	explicit–implicit
M-DI ($\beta = 1$)	Modified Direct-Implicit, Eqs. (3.17)–(3.21) with $\beta = 1$ and $\phi^0 = 0$	implicit

where β is a parameter which controls the degree of implicitness ($0 \leqslant \beta \leqslant 1$) and $\widetilde{\phi}^{m+1}$ is a temporary potential which will be defined below. Then, temporary densities $\widetilde{n}_{i,e}^{m+1}$ are assigned from the particle positions $(\widetilde{X}_{i,e})_j^{m+1}$ and the electric field at time t^{m+1} is given by the following implicit correction to the explicit electric field:

$$(\overline{E}_{i,e})_j^{m+1} = (1-\beta)(\overline{E}_{i,e})_j^m - \beta \nabla \phi^{m+1}((\widetilde{X}_{i,e})_j^{m+1}), \tag{3.20}$$

where ϕ^{m+1} is a correction to $\widetilde{\phi}^{m+1}$ and is a solution to the equation:

$$-\nabla \cdot \left(\left((\Delta t)^2 \beta (\widetilde{n}_i^{m+1} + \frac{\widetilde{n}_e^{m+1}}{\varepsilon}) + \lambda^2 \right) \nabla \phi^{m+1} \right) = \widetilde{n}_i^{m+1} - \widetilde{n}_e^{m+1} - \nabla \cdot \left((\Delta t)^2 \beta \left(\widetilde{n}_i^{m+1} + \frac{\widetilde{n}_e^{m+1}}{\varepsilon} \right) \nabla \widetilde{\phi}^{m+1} \right). \tag{3.21}$$

Finally, the particle positions and velocities are updated with the classical "leap-frog scheme" from the positions $(X_{i,e})_j^m$ and velocities $(V_{i,e})_j^m$ at time t^m, in the partly implicit electric field $(\overline{E}_{i,e})_j^{m+1}$.

The temporary potential $\widetilde{\phi}^{m+1}$ can be chosen in various ways. In the following numerical simulations, it is chosen equal to 0. An other possible choice is $\widetilde{\phi}^{m+1} = \phi^m$. Simulations using the latter have been carried out in the present work but did not give rise to significant improvements compared to the former (and even sometimes provided mildly unstable results). For this reason, only simulation results using $\widetilde{\phi}^{m+1} = 0$ will be shown.

In the following, we will consider the explicit–implicit Direct-Implicit method with $\beta = 1/2$: it will be called the Classical Direct-Implicit method and denoted C-DI ($\beta = 1/2$). The first iterate of the scheme requires the computation of the initial potential via the classical Poisson equation (2.7) (to provide both the velocities $V_j^{1/2} \approx V_j(\Delta t/2)$ and the initial explicit electric field). As shown in the numerical simulations, instabilities can then be generated in under-resolved case. That is why we consider two modified Direct-Implicit schemes: Modified DI ($\beta = 1/2$) and Modified DI ($\beta = 1$) denote Direct-Implicit schemes where the initial potential is zero. Modified DI ($\beta = 1/2$) is an explicit–implicit Direct-Implicit scheme while Modified DI ($\beta = 1$) is a fully implicit Direct-Implicit scheme.

We note that (3.21) is consistent with the Poisson equation when $\Delta t \to 0$ for fixed λ. On the other hand, when $\lambda \to 0$ with fixed Δt, the resulting equation is

$$-\nabla \cdot \left((\Delta t)^2 \beta \left(\widetilde{n}_i^{m+1} + \frac{\widetilde{n}_e^{m+1}}{\varepsilon} \right) \nabla \phi^{m+1} \right) = \widetilde{n}_i^{m+1} - \widetilde{n}_e^{m+1} - \nabla \cdot \left((\Delta t)^2 \beta \left(\widetilde{n}_i^{m+1} + \frac{\widetilde{n}_e^{m+1}}{\varepsilon} \right) \nabla \widetilde{\phi}^{m+1} \right).$$

When $\Delta t \to 0$, this scheme leads to

$$\widetilde{n}_i^{m+1} - \widetilde{n}_e^{m+1} = 0, \tag{3.22}$$

which does not provide any equation for ϕ^{m+1}. Additionally, since $\widetilde{n}_i^{m+1}$ and $\widetilde{n}_e^{m+1}$ do not depend on ϕ^{m+1}, there is no way ϕ^{m+1} can be adjusted in such a way that the constraint (3.22) can be matched. In other words, the scheme (3.21) is not Asymptotic-Preserving in the sense of the definition stated in Section 1.

We refer to [31,32] for a more thorough presentation of the Direct-Implicit schemes and to Table 1 for a summary of the definition of the different schemes.

4. Numerical results

In this section we show numerical results in one space dimension for the Vlasov–Poisson system. We simulate four test-cases and we compare the results obtained with the Classical PIC, PICAP-1 and PICAP-2 schemes. Simulations with the Direct-Implicit schemes, C-DI ($\beta = 1/2$), M-DI ($\beta = 1/2$) and M-DI ($\beta = 1$), are also performed in most of the test-cases.

The first test-case consists in a steady state, the second test-case is a bump-on-tail instability, the third test-case is a perturbation of a Maxwellian plasma and the fourth test-case is a plasma expansion in vacuum.

4.1. Steady state test-case

The first test case is dedicated to the study of the damping resulting from the implicitness of the PICAP schemes in the case of a steady state and they are compared to the Direct-Implicit schemes. We initialize the Vlasov–Poisson equation with the following steady state: the ion are supposed motionless and the distribution function of electrons is uniform,

$$f_0(x,v) = (2\pi)^{-\frac{1}{2}} \exp(-v^2/2), \quad n_0 = 1, \tag{4.1}$$

on the domain (0,1). We consider periodic boundary conditions for the Vlasov equation and homogeneous Dirichlet boundary conditions for the Poisson equation. The Debye length is chosen equal to $\lambda = 10^{-3}$ and thus the plasma period is $\omega^{-1} = 10^{-3}$.

In Fig. 1, we consider a resolved case: $\Delta x = 10^{-4} < \lambda$. The time-step is chosen such as it satisfies the CFL conditions: $v_{\max}\Delta t = 0.9\Delta x$, where $v_{\max}$ is the maximal electron velocity at each time-step. As a consequence, time scales are also resolved: $\omega\Delta t \leqslant 1$. We use 100 particles per cell. Fig. 1 shows the total energy as function of time. For the exact solution of the Vlasov–Poisson equation (one-species case), the total energy $\mathcal{E}$ is given by

$$\mathcal{E} = \frac{\lambda^2}{2}\int |\partial_x \phi|^2 dx + \frac{1}{2}\int f|v|^2\, dx\, dv, \tag{4.2}$$

and is constant in time. The Classical PIC and the Classical Direct-Implicit schemes preserve the total energy while the PICAP-1, PICAP-2 and M-DI ($\beta = 1$) schemes damp it since they are fully implicit. The damping rates related to these schemes are reported in Table 2, Minimizing this damping effect by combining explicit and implicit computations is the goal of the vast literature about Direct-Implicit schemes [31,32]. PICAP schemes seem more dissipative but further studies about second order time-stepping strategies may improve this feature.

Fig. 2 presents results for the under-resolved case $\Delta x = 10^{-1} > \lambda$, where $\lambda = 10^{-3}$ is unchanged. For Classical PIC and Classical DI ($\beta = 1/2$) schemes, we use a uniform time-step $\Delta t = 15\omega^{-1}$, since the CFL conditions would be too restrictive due to

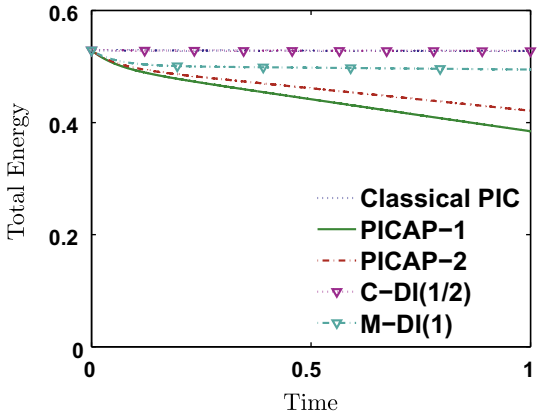

Fig. 1. Steady state in the resolved case: $\Delta x = 10^{-4} < \lambda = 10^{-3}$ and $\Delta t < \omega^{-1} = 10^{-3}$. Total energy as a function of scaled time with Classical PIC, PICAP-1, PICAP-2, Classical DI ($\beta = 1/2$) and Modified DI ($\beta = 1$) schemes.

Table 2
Damping rates.

PICAP-1	PICAP-2	M-DI ($\beta = 1$)
−27%	−20%	−6.5%

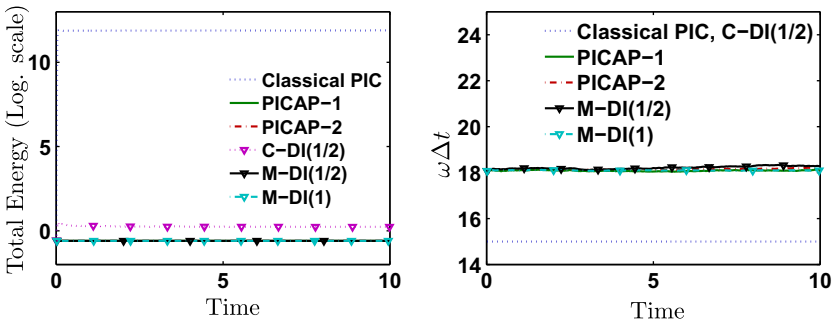

Fig. 2. Steady state in the under-resolved case: $\Delta x = 10^{-1} > \lambda = 10^{-3}$ and $\Delta t > \omega^{-1} = 10^{-3}$. Total energy in log scale (left) and $\omega\Delta t$ (right) as a function of scaled time with Classical PIC, PICAP-1, PICAP-2, Classical DI ($\beta = 1/2$), Modified DI ($\beta = 1/2$) and Modified DI ($\beta = 1$) schemes.

the large particle velocities induced by the instability. For the other schemes, the time-step is given by the CFL condition $v_{\max}\Delta t = 0.9\Delta x$. Fig. 2(right) shows that time is under-resolved for all the schemes. We consider now 10^5 particles per cell in order to have the same total number of particles as in the resolved case. Total energies are plotted in Fig. 2(left) for the different schemes (Classical PIC, PICAP-1, PICAP-2, Classical DI ($\beta = 1/2$), Modified DI ($\beta = 1/2$) and Modified DI ($\beta = 1$)). We note that the Classical PIC and Classical DI ($\beta = 1/2$) methods are unstable: unphysically large electrical energies are reached after the first time step. The other schemes (PICAP-1, PICAP-2, Modified DI ($\beta = 1/2$), Modified DI ($\beta = 1$)) damp the energy. The damping rate is approximately of the same order and is about -0.01%. Since the number of particles per cell is larger than previously and the time-step bigger, the dissipation due to the particle-grid assignment-interpolation procedure is lower.

4.2. Periodic perturbation of a quasineutral Maxwellian plasma

In this section, we investigate the dynamics of a small perturbation of a Maxwellian plasma (see also [13]). We perform the simulation on the domain $(0,1)$ with periodic boundary conditions for the Vlasov system and with homogeneous Dirichlet boundary conditions for the Poisson equation.

We consider successively the one-species case (i.e. system (2.8) and (2.9)) and the two-species case (i.e. system (2.5)–(2.7)). In [13], only the one-species case was considered. In the two-species case, we choose a realistic mass ratio $\varepsilon = 10^{-4}$. The PICAP schemes seem robust even in the case of realistic electron to ion mass ratios. However, ideally, an Asymptotic-Preserving scheme for both the limits $\lambda \to 0$ and $\varepsilon \to 0$ should be sought. This problem is under current investigation.

4.2.1. Periodic perturbation: one species case

For this case, we develop the PICAP-1 and PICAP-2 schemes for system (2.8) and (2.9). We select $\lambda = 10^{-4}$ which means that the scaled plasma frequency has the value $\omega = \frac{1}{\lambda} = 10^4$ and we use 100 particles per cell. We initialize the Vlasov–Poisson equation with

$$f_0 = \pi^{-1/2}(1 + \delta \sin(\kappa\pi x)) \exp(-v^2), \quad n_0 = 1. \tag{4.3}$$

where $\delta = 10^{-2}$ is the perturbation amplitude and $\kappa = 2220$. The value of κ is chosen such that $\kappa \sim \lambda^{-1}$ to ensure that the wavelength of the density perturbation is of the same order as the Debye length. In this case, the phase velocity of the wave (which is nearly ω_p/κ in physical units) is of the same order as the thermal velocity v_{th} (which in our dimensionless units, is unity). This situation corresponds to a strong particle-wave coupling [7,30], since the thermal velocity roughly coincides with the location of the steepest slope of the velocity distribution function.

In Fig. 3, we present results obtained with the Classical PIC, PICAP-1 and PICAP-2 schemes when $\Delta x = \lambda = 10^{-4}$. The time step Δt satisfies both CFL conditions $v_{\max}\Delta t \leqslant \Delta x$ and $\omega\Delta t \leqslant 1$. In these conditions, the fast space and time scales (respectively the Debye length and plasma period) are both resolved. Fig. 3(left) gives the electric potential as a function of position at an instant $t = 10\omega^{-1} = 10^{-3}$. The electric potential is almost identical with the three schemes. The electric potential as a function of position is shown in Fig. 3(right) after a large number of plasma periods ($t = 2000\omega^{-1} = 0.2$). We can see that the amplitude of the plasma waves is of the same order of magnitude as previously when using the Classical PIC scheme, while it has been strongly damped out with the PICAP-1 and PICAP-2 methods. This shows that the AP strategy damps out the energy of the plasma waves and allows to capture phenomena which occur on longer time scales. In other words, the AP discretization of the Vlasov–Poisson problem damps out the plasma waves. On the other hand, waves that exist in quasineutral conditions (such as ion-acoustic or Alfven waves) should not be altered by the AP procedure. Indeed, the simulations of the ion slab expansion (see Section 4.4) show that the model gives a correct account of the expansion, which propagates at about the ions acoustic wave-speed.

Fig. 4 now shows the results obtained when the fast space and time scales are both under-resolved, i.e. the space step is larger than the Debye length $\Delta x > \lambda$ and the time-step is larger that the plasma period $\Delta t > \omega^{-1}$. We choose $\Delta x = 10^{-2}$ while

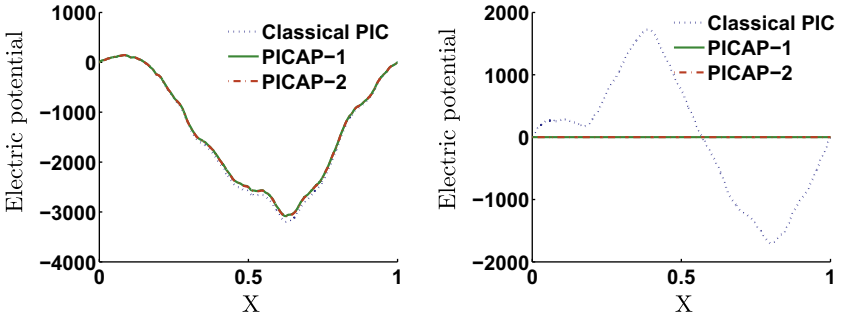

Fig. 3. One-species periodic perturbation of a quasi-neutral Maxwellian plasma, resolved case: $\Delta x = \lambda = 10^{-4}$ and $\Delta t < \omega^{-1} = 10^{-4}$. Electric potential as a function of position, with Classical PIC, PICAP-1 and PICAP-2 schemes. Left: at scaled time $t = 10\omega^{-1} = 10^{-3}$ (all curves are identical); right: at scaled time $t = 0.2 = 2000\omega^{-1}$.

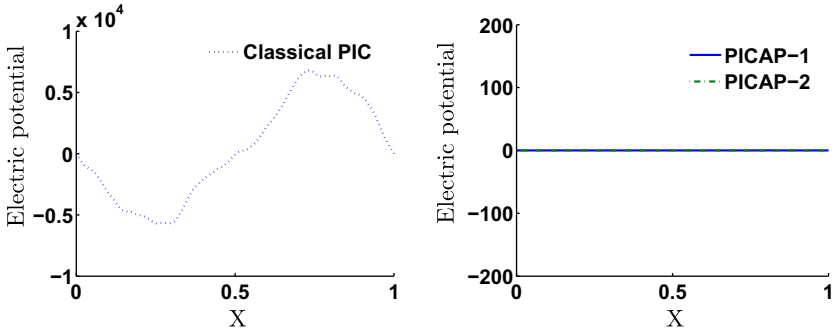

Fig. 4. One-species periodic perturbation of a quasi-neutral Maxwellian plasma, under-resolved case: $\Delta x = 10^{-2} > \lambda = 10^{-4}$ and $\Delta t > \omega^{-1} = 10^{-4}$. Electric potential as a function of position, with Classical PIC scheme (left), and PICAP-1, PICAP-2 schemes (right), at scaled time $t = 0.2 = 2000\omega^{-1}$.

$\lambda = 10^{-4}$ is unchanged. Meanwhile, the total number of particles is kept unchanged. For both PICAP-1 and PICAP-2 schemes, we use a time-step determined by the CFL conditions: $v_{\max}\Delta t \leqslant \Delta x$. In Fig. 6, we plot $\omega\Delta t$ as a function of time. We see that this constraint still allows Δt of the order of 30 times the plasma period ω^{-1}. Simultaneously, we use a uniform time-step for the Classical PIC scheme, with $\Delta t = 30\omega^{-1}$. We cannot use the CFL condition because the instability generates very large particle velocities and enforcing the CFL condition would generate very small time-steps.

Fig. 4 depicts the electric potential as a function of space, at time $t = 0.2$. The left picture shows a result using the classical PIC scheme. The instability of the scheme is clearly visible since the amplitude of the potential oscillations are now of the order of ten times those of the initial potential (see Fig. 3 for instance). With the PICAP-1 or PICAP-2 schemes, these amplitudes are now very small showing that the schemes are stable and have damped out plasma waves, as in the resolved case.

Fig. 5 displays the total energy $\mathcal{E}$ (in log scale) as a function of time for the different schemes in the resolved and under-resolved situations. Fig. 5(left) shows the resolved case. We notice that the total energy for the Classical PIC scheme decays slowly after a more rapid initial transient. By contrast, the total energy of both PICAP-1 and PICAP-2 schemes decays more steadily. In Fig. 5(right), the under-resolved case is considered. With the Classical PIC scheme, the total energy is unstable and reaches large and totally unrealistic values after a very rapid initial transient. With the AP schemes, they are both stable and damped to zero. We note that the PICAP-2 scheme seems to exhibit a slower energy decay than the PICAP-1 scheme which has been initially proposed in [13]. Paradoxically, the energy decay of the PICAP-1 and PICAP-2 seems far less pronounced in the under-resolved case than in the resolved case, probably because the number of assignment-interpolation procedures per unit time has been reduced, leading to a lower diffusive scheme.

In [13], the energy damping has been attributed to the noisy coefficients of the reformulated Poisson equation (3.12) (because the densities and the tensors S have to be computed from the particles and because additionally, a second order space derivative of S is needed as a source term in this equation). It has been noticed that, if high frequencies are cut off in order to eliminate the noise, the energy damping can be significantly reduced. The application of filtering techniques, or more generally, of noise reduction techniques to these new PICAP schemes will be the subject of future studies.

When the fast space scale is under-resolved but the fast time scale is resolved, the Classical PIC scheme is still unstable. We have performed simulations with $\Delta x = 10^{-2}$, $\lambda = 10^{-4}$ and $\Delta t = 0.9\omega^{-1}$. The results are very similar to those obtained in the fully (time and space) under-resolved case (and for this reason, the results are not displayed). This is to be compared to the behaviour of classical schemes for the fluid models (i.e. the Euler–Poisson problem in the quasineutral limit) [12], where it has been observed that the results are stable as long as the fast time scale is resolved, even if the fast space scale is under-resolved. It looks as if the kinetic problem was more unstable than the fluid one, since as soon as one of the fast time or space

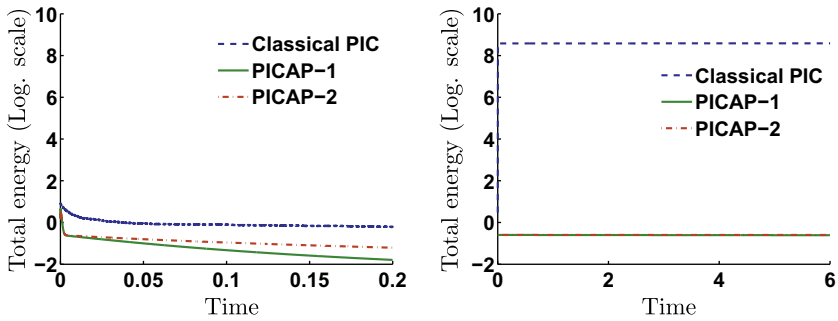

Fig. 5. One-species periodic perturbation of a quasi-neutral Maxwellian plasma, with $\lambda = 10^{-4}$, $\omega = 10^4$: total energy in log scale as a function of scaled time, with Classical PIC, PICAP-1 and PICAP-2 schemes. Left: resolved case: $\Delta x = \lambda$ and $\Delta t < \omega^{-1}$; right: under-resolved case: $\Delta x = 10^{-2} > \lambda$ and $\Delta t > \omega^{-1}$.

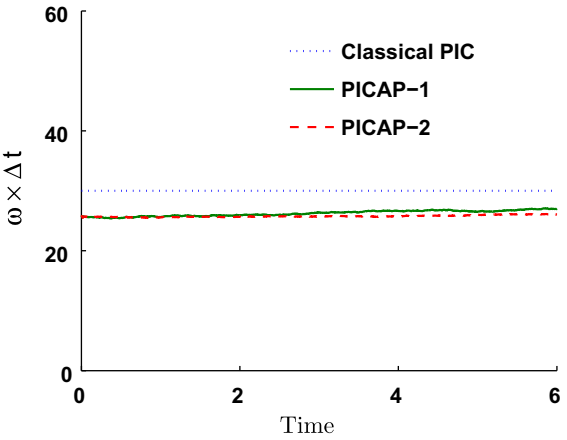

Fig. 6. One-species periodic perturbation of a quasi-neutral Maxwellian plasma, under-resolved case: $\Delta x = 10^{-2} > \lambda = 10^{-4}$ and $\Delta t > \omega^{-1} = 10^{-4}$. $\omega\Delta t$ as a function of scaled time, with Classical PIC, PICAP-1 and PICAP-2 schemes.

scale is under-resolved, the scheme becomes unstable. By contrast, both the PICAP-1 and PICAP-2 schemes are stable. The results are very similar to those of the fully resolved case and are not represented.

4.2.2. Periodic perturbation: two species case

In this section, we consider the two species problem (2.5)–(2.7) and choose the following parameters:

$$\varepsilon = 10^{-4}, \quad \lambda = 10^{-4} \quad \left(\omega = \frac{1}{\lambda\sqrt{\varepsilon}} = 10^{6}\right).$$

Again, we put 100 ions and 100 electrons in each cell. We initialize this test-case with

$$f_{e0} = \varepsilon\pi^{-1/2}(1 + \delta\sin(\kappa\pi x))\exp(-\varepsilon v^2),$$
$$f_{i0} = \pi^{-1/2}(1 + \delta\sin(\kappa\pi x))\exp(-v^2)$$

with $\delta = 10^{-2}$ and $\kappa = 2220$.

We successively consider the case where the Debye length and electron plasma period are both resolved ($\Delta x = \lambda$, $\Delta t < \omega^{-1}$, Δt satisfying the CFL condition $v_{\max}\Delta t \leqslant \Delta x$), and where none of the Debye length and plasma period are resolved. In the latter case, the time-step is chosen to satisfy the CFL condition: $\Delta t = 0.9\Delta x/v_{\max}$. Fig. 8 shows the evolution of the time-step as a function of time. We notice that the time-step reaches values which are of the order of *25* times the plasma period. For the standard PIC scheme, the time-step is kept fixed at this value for the same reason as explained above. We observe that the PICAP methods damp plasma waves in a similar way as in the one-species cases, and that they provide stable computations in the under-resolved case, while, in the latter case, the Classical PIC is unstable. We omit the corresponding pictures as they are similar to Figs. 3 and 4. We only display the total energy as a function of time.

In the two-species case, the total energy of the Vlasov–Poisson problem is given by

$$\mathcal{E} = \frac{\lambda^2}{2}\int |\partial_x\phi|^2\,dx + \frac{1}{2}\int f_i|v|^2\,dx\,dv + \frac{\varepsilon}{2}\int f_e|v|^2\,dx\,dv, \tag{4.4}$$

and is constant in time. The total energy (in log scales) as a function of time is displayed in Fig. 7, in the resolved case (left) and under-resolved one (right). The conclusions are the same as in the one-species case: the energy dissipation of the Classical PIC scheme is lower than that of the two AP schemes in the resolved case. However, in the under-resolved case, the Classical PIC scheme exhibits a severe instability while the two AP schemes are still stable. Additionally, the energy dissipations of the AP schemes in the under-resolved case are slightly less pronounced than in the resolved case. In this two-species case, the two AP schemes seem to behave similarly as regards the energy dissipation properties and the lower energy dissipation of PICAP-2 compared with PICAP-1 is less apparent.

These results confirm that, in a situation where standard PIC methods would be unstable, the PICAP schemes remain stable and dissipate the electric energy of the plasma waves.

4.2.3. Linear Landau damping test-case

In this section, the PICAP-1 and PICAP-2 schemes are compared to both the Direct-Implicit scheme [31,32] and the Eulerian solver used in [2]. The frequency κ of the density perturbation is of order one. The target of such a test case is to measure the accuracy of the numerical schemes for capturing nonlinear Landau damping, which is a phenomenon occurring on the time scales of the plasma oscillations. So as to perform comparisons, we initialize the Vlasov–Poisson equation as in [2]:

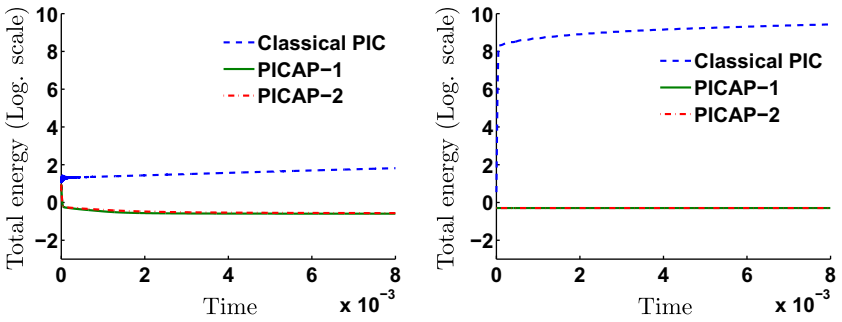

Fig. 7. Two-species periodic perturbation of a quasi-neutral Maxwellian plasma, $\varepsilon = 10^{-4}$, $\lambda = 10^{-4}$, $\omega = 10^6$: total energy (in log scales) as a function of scaled time, with Classical PIC scheme, PICAP-1 and PICAP-2 schemes. Left: resolved case: $\Delta x = \lambda$ and $\Delta t < \omega^{-1}$ ($\Delta t = 0.9\Delta x/v_{max}$); right: under-resolved case: $\Delta x = 10^{-2} > \lambda$ and $\Delta t > \omega^{-1}$ ($\Delta t = 0.9\Delta x/v_{max} \approx 25\omega^{-1}$).

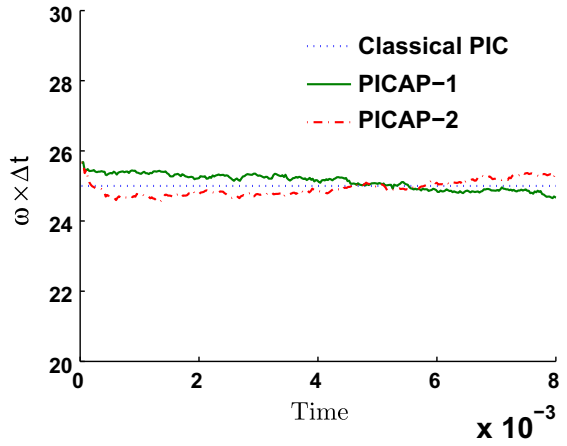

Fig. 8. Two-species periodic perturbation of a quasi-neutral Maxwellian plasma, under-resolved case: $\Delta x = 10^{-2} > \lambda$ and $\Delta t > \omega^{-1}$, $\varepsilon = 10^{-4}$, $\lambda = 10^{-4}$, $\omega = 10^6$. $\omega\Delta t$ as a function of scaled time, with Classical PIC, PICAP-1 and PICAP-2 schemes.

$$f_0 = (2\pi)^{-\frac{1}{2}}(1 + \delta\sin(\kappa x))\exp(-v^2/2), \quad n_0 = 1, \tag{4.5}$$

on the interval $(0, 2\pi/\kappa)$. The perturbation amplitude is taken equal to $\delta = 10^{-2}$ and $\kappa = 1$. We take $\Delta x = 2 \times 10^{-2}$ and we consider 10^4 particles per cell (in average). Thus, the total number of particles is of the same order as in the previous test case.

Fig. 9 shows results for a resolved case $\lambda = 1 > \Delta x = 2 \times 10^{-2}$. The time-step is chosen such that the CFL condition $v_{\max}\Delta t = 0.9\Delta x$ is satisfied. As a consequence, time scales are also resolved: $\omega\Delta t \leqslant 1$. Fig. 9(left) depicts the norm of the

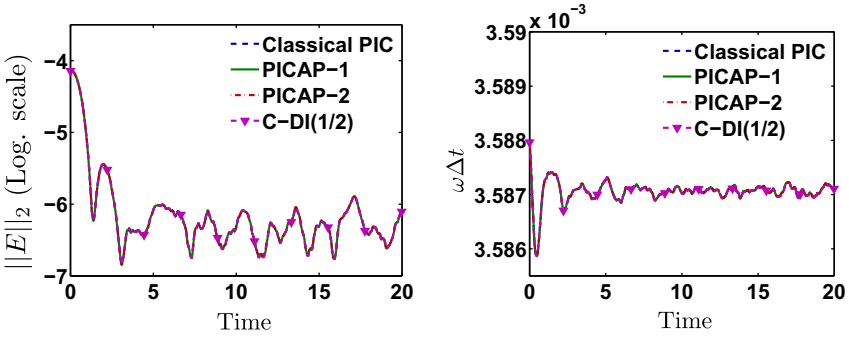

Fig. 9. Linear Landau damping in the resolved case: $\Delta x = 2 \times 10^{-2} < \lambda = 1$ and $\Delta t < \omega^{-1} = 1$. Left: norm of the electric field in log scale as a function of scaled time with Classical PIC, PICAP-1, PICAP-2 and Classical DI ($\beta = 1/2$) schemes. Right: $\omega\Delta t$ as a function of scaled time, with Classical PIC, PICAP-1, PICAP-2 and Classical DI ($\beta = 1/2$) schemes. This picture must be compared with Fig. 5 of Ref. [2].

electric field (in log scale) as a function of time obtained with the Classical PIC, PICAP-1, PICAP-2 and classical Direct-Implicit schemes. In Fig. 9(right), $\omega\Delta t$ as function of time is plotted. The four schemes give identical results. The measured slope is about 0.64, which has the same order as the theoretical one (see Ref. [2, Fig. 3]). However, due to the noise which is inherent to particles simulations, this value is not as precise as for semi-Lagrangian simulations. For the same reason, the damping is stopped at $t \simeq 4\omega^{-1}$ instead of going on.

In Fig. 10, we present the results for an under-resolved case: $\lambda = 10^{-4} < \Delta x$ and $\omega^{-1} = 10^{-4} < \Delta t$. The space step $\Delta x = 2 \times 10^{-2}$ is unchanged. For the Classical PIC and the Classical DI ($\beta = 1/2$) schemes, we use a uniform time-step $\Delta t = 30\omega^{-1}$. For the other schemes, the time-step is determined by the CFL conditions: $v_{\max}\Delta t = 0.9\Delta x$. Fig. 10 shows the norm of the electric field (in log scale) as a function of time for the different schemes. As in the previous test case, the Classical PIC is unstable. The Direct-Implicit scheme seems also unstable but the stable results given by the Modified DI ($\beta = 1/2$) and Modified DI ($\beta = 1$) schemes prove that it is essentially due to the computation of the first time-step. Finally, the Modified DI ($\beta = 1/2$) and the Modified DI ($\beta = 1$) schemes provide similar results to those of the PICAP-1 and PICAP-2 schemes. These results are not comparable to those obtained in [2]. This is because plasma oscillations are not resolved at all in this situation and none of the tested schemes is able to provide a reliable estimate of the damping rate. Both Direct-Implicit and PICAP methods provide an over-damping of the plasma waves. In Fig. 10(right), we plot $\omega\Delta t$ as a function of time. We see that the damping of the wave by the PICAP-1, the PICAP-2, the Modified DI ($\beta = 1/2$) and the modified DI ($\beta = 1$) schemes results in increased time-steps.

4.3. Bump-on-tail test-case

In this section, we compare the AP methods to the Classical PIC scheme and the Direct-Implicit method in the case of a bump-on-tail instability, which is a form of the two-stream instabilities. The results must be also compared with those obtained with an Eulerian code in [2]. We initialize the Vlasov–Poisson equation with

$$f_0(x, v) = f_1(v)(1 + \delta\cos(\kappa x)), \tag{4.6}$$

where the function f_1 is given by:

$$f_1(v) = C\Big(\exp(-v^2/2) + \alpha\exp(-(v - v_d)^2/2v_t^2)\Big), \tag{4.7}$$

where C is a renormalization constant. Periodic boundary conditions for the Vlasov–Poisson system and homogeneous Dirichlet boundary conditions for the Poisson equations are considered. The numerical parameters are $\alpha = 0.04$, $\kappa = 0.3$, $v_d = 4.5$, $v_t = 0.5$ and $\alpha = 2/9$, and are those chosen in [2]. The space domain is $(0,20\pi)$ and we consider periodic boundary conditions.

Fig. 11(left) shows results for a very resolved case, where $\lambda = 1$ and $\Delta x = 2.10^{-3}$. We consider 10 particles per cell (in average). We consider also a CFL condition like $\Delta t = 0.9\Delta x/v_{\max}$, which consequently ensures the resolution of time scales. Electrostatic energy is plotted in Fig. 11(left) for Classical PIC, PICAP-1, PICAP-2 and Classical Direct-Implicit schemes. It should be compared with Fig. 10 of [2]. The various schemes are in very good agreement one with each other up to time $100\omega^{-1}$. Besides, up to time $50\omega^{-1}$, they are also in good agreement with the result obtained in [2]. After time $50\omega^{-1}$, the results are altered by the damping due to the numerical noise of PIC methods. However, all the schemes capture the dynamics well, despite the small number of particles per cell.

We consider now the following under-resolved case: $\Delta x = 3$ while $\lambda = 10^{-1}$. We consider 6.10^4 particles per cell (in average). For the Classical PIC and the Classical DI ($\beta = 1/2$) schemes, we enforce the condition $\Delta t = 4\omega^{-1}$ to be sure that time is under-resolved. For the PICAP-1, the PICAP-2, the Modified DI ($\beta = 1/2$) and the Modified DI ($\beta = 1$) schemes, the time-step is computed from the CFL conditions $v_{\max}\Delta\ t = 0.9\Delta x$. Fig. 12(right) shows that time scales are under-resolved for all these

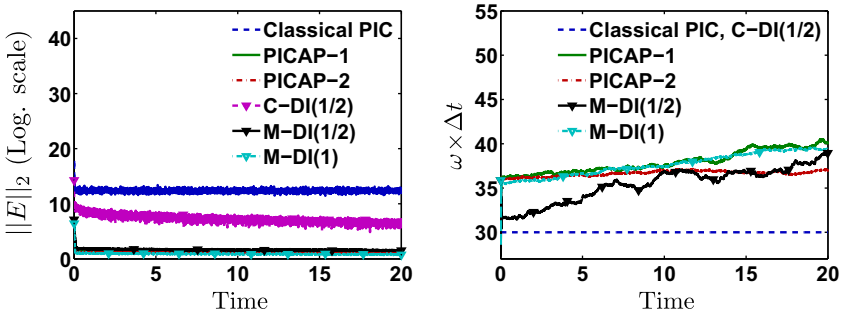

Fig. 10. Linear Landau damping in the under-resolved case: $\Delta x = 2 \times 10^{-2} > \lambda = 10^{-4}$ and $\Delta t > \omega^{-1} = 10^{-4}$. Left: norm of the electric field in log scale as a function of scaled time with Classical PIC, PICAP-1, PICAP-2, Classical DI ($\beta = 1/2$), Modified DI ($\beta = 1/2$) and Modified DI ($\beta = 1$) schemes. Right: $\omega\Delta t$ as a function of scaled time with Classical PIC, PICAP-1, PICAP-2, Classical DI ($\beta = 1/2$), Modified DI ($\beta = 1/2$) and Modified DI ($\beta = 1$) schemes. This picture must be compared with Fig. 17 of Ref. [2].

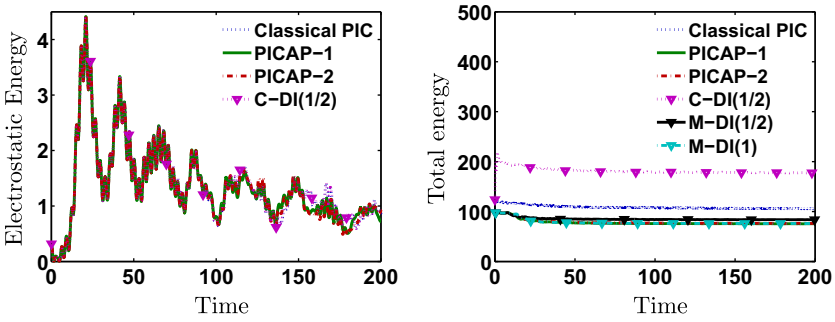

Fig. 11. Bump on tail instability. Left: electrostatic energy as a function of scaled time with Classical PIC, PICAP-1, PICAP-2 and Classical DI ($\beta = 1/2$) schemes, in the resolved case: $\Delta x = 2 \times 10^{-3} < \lambda = 1$ and $\Delta t > \omega^{-1} = 1$. Right: comparison of methods: total energy as a function of scaled time, in the resolved case $\Delta x = 5 \times 10^{-2} < \lambda = 10^{-1}$ for Classical PIC scheme and in the under-resolved case $\Delta x = 3 > \lambda = 10^{-1}$ for PICAP-1, PICAP-2, Classical DI ($\beta = 1/2$), Modified DI ($\beta = 1/2$), Modified DI ($\beta = 1$) schemes. These pictures must be compared with Figs. 10 and 15 of Ref. [2].

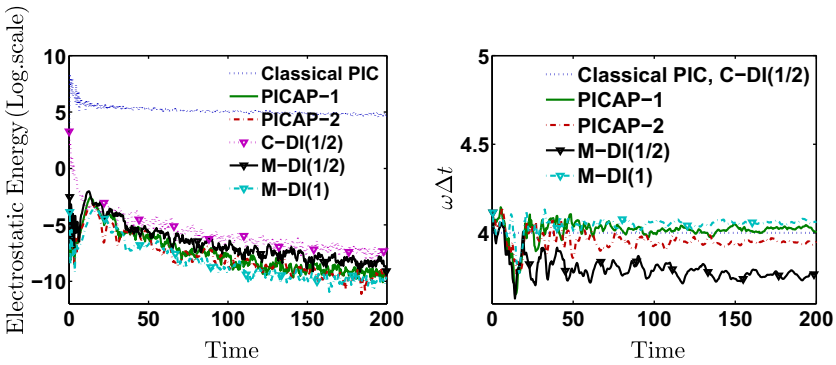

Fig. 12. Bump on tail instability. Right: electrostatic energy in log scale as a function of scaled time with Classical PIC, PICAP-1, PICAP-2, Classical DI ($\beta = 1/2$), Modified DI ($\beta = 1/2$) and Modified DI ($\beta = 1$) schemes, in the under-resolved case: $\Delta x = 3 > \lambda = 10^{-1}$ and $\Delta t > \omega^{-1} = 10^{-1}$. This picture must be compared with Fig. 13 of Ref. [2]. Left: $\omega\Delta t$ as a function of scaled time with Classical PIC, PICAP-1, PICAP-2, Classical DI ($\beta = 1/2$), Modified DI ($\beta = 1/2$) and Modified DI ($\beta = 1$) schemes, in the under-resolved case: $\Delta x = 3 > \lambda = 10^{-1}$ and $\Delta t > \omega^{-1} = 10^{-1}$.

schemes since $\Delta t \simeq 4\omega^{-1}$ for all the schemes. In Fig. 12(left), electrostatic energy is plotted for Classical PIC, PICAP-1, PICAP-2, Classical Direct-Implicit, Modified DI ($\beta = 1/2$) and Modified DI ($\beta = 1$) schemes: while Classical PIC exhibits a large instability before damping, Classical DI ($\beta = 1/2$) and Modified DI ($\beta = 1/2$) rapidly damp the energy but not as much as PICAP-1 and PICAP-2. Fig. 13 displays the electron velocity distribution function for the different schemes at time $t = 0$, 200, 300 and $2000\omega^{-1}$. Classical PIC does not give coherent results: all the particles have large velocities. Classical DI ($\beta = 1/2$) strongly heats up the system since the number of particles with small velocities decreases strongly. The Modified DI ($\beta = 1/2$) scheme does not seem unstable. However, among the last four schemes, it gives rise to the larger number of particles with fast velocities (see at $v = 6$). On the contrary, the Modified DI ($\beta = 1$) scheme seems to produce the system with the largest number of particles with small velocities (see at $v = 2$). The PICAP methods provide intermediate results. All these results are similar to those presented in Fig. 14 of [2]. Moreover, the results obtained with the PICAP-1, PICAP-2, Classical Direct-Implicit, Modified DI ($\beta = 1/2$) and Modified DI ($\beta = 1$) schemes are in concordance with the resolved case considered in Fig. 12 of [2].

So as to compare the loss of energy due to the numerical schemes, Fig. 11(right) shows the total energy with the resolved Classical PIC scheme (with $\lambda = 10^{-1}$, $\Delta x = 5 \cdot 10^{-2}$ and 10^3 particles per cell) and with the under-resolved other schemes (with $\lambda = 10^{-1}$, $\Delta x = 3$ and $6 \cdot 10^4$ particles per cell). As in the steady state test case, we can observe that fully implicit schemes (PICAP-1,PICAP-2 and Modified DI ($\beta = 1$)) damp energy approximately at the same level and more rapidly than the explicit–implicit schemes, i.e. the Classical DI ($\beta = 1/2$) and the Modified DI ($\beta = 1/2$) schemes. Comparisons with Fig. 15 of [2] show that the damping due to the interpolation-assignment procedure of PIC methods seems to be more important than the damping due to implicitness.

4.4. One-dimensional plasma expansion test-case

4.4.1. Setting of the problem

We consider a one-dimensional plasma expansion problem which is described in [22,23]. This is a two-species problem where the ions initially occupy a slab of thickness L, while the electrons are initialized by a Maxwell–Boltzmann equilibrium with a self-consistent potential. The test problem consists in observing the expansion of the ion slab.

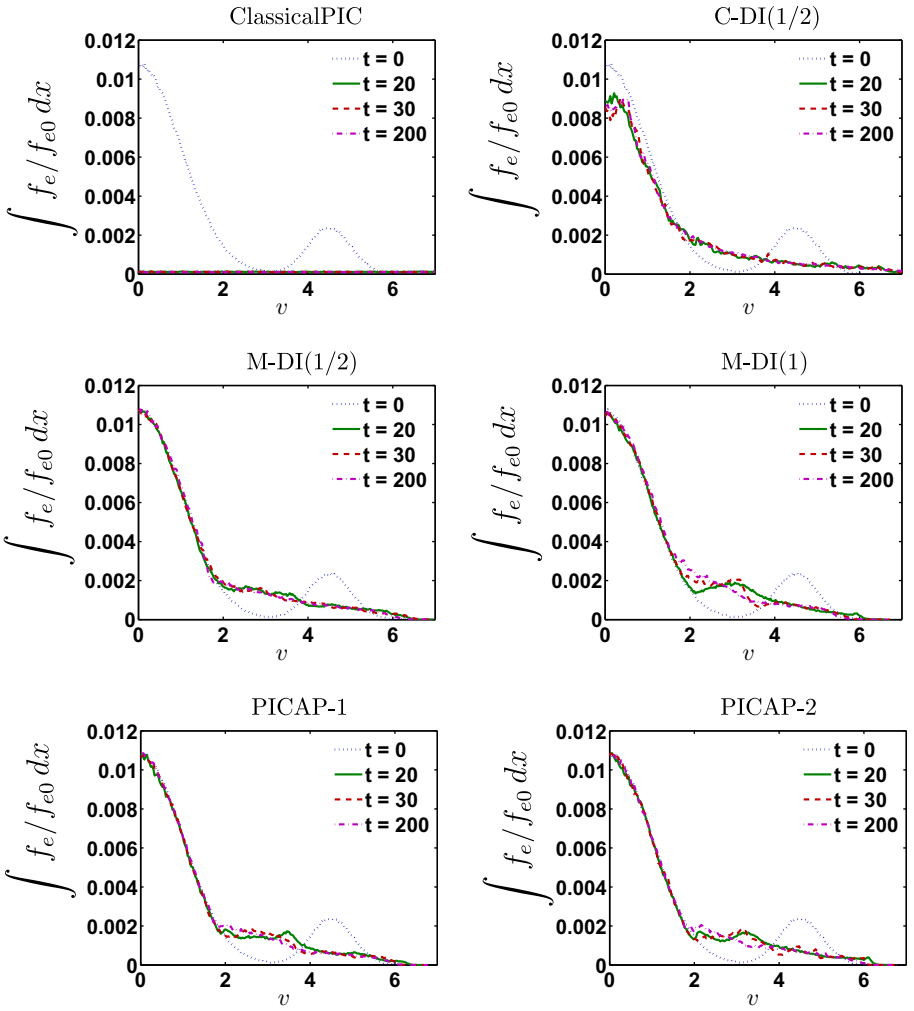

Fig. 13. Bump on tail instability in the under-resolved case: $\Delta x = 3 > \lambda = 10^{-1}$ and $\Delta t > \omega^{-1} = 10^{-1}$. Left top: velocity distribution function as a function of velocity with Classical PIC scheme. Right top: velocity distribution function as a function of velocity with Classical DI ($\beta = 1/2$). Left medium: velocity distribution function as a function of velocity with Modified DI ($\beta = 1/2$) scheme. Right top: velocity distribution function as a function of velocity with Modified DI ($\beta = 1$) scheme. Bottom left: velocity distribution function as a function of velocity with PICAP-1 scheme. Bottom right: velocity distribution function as a function of velocity with PICAP-2 scheme.

The initial electron temperature is 1000 times higher than the initial ion temperature. The simulation box is $[0,A]$ and the ions are initialized in $[0,L/2]$ with $L/2 \ll A$ (for reasons of symmetry, only half of the domain is simulated and a symmetry axis is set at $x = 0$). The mass ratio is $\varepsilon = 1/1836$. We scale the energies according to the electron thermal energy, using $\bar{\phi} = e\phi/(k_B T_{e0})$, $v_0 = k_B T_{e0}/m_i$ in (2.4). The scaled Vlasov–Poisson system is the same as before: (2.5)–(2.7). The boundary conditions for the potential are

$$\phi(0) = 0, \quad \partial_x \phi(A) = 0. \tag{4.8}$$

To enforce that $x = 0$ is an axis of symmetry, we assume specular reflection for the distribution function (i.e. particles are reinjected with reversed velocities), while the right boundary is a purely absorbing one, i.e. particles exiting the domain at $x = A$ are free to leave it while no particle is reinjected.

The initial electron density is defined by the Boltzmann relation

$$n_{e0} = n_0 \exp \phi_0, \tag{4.9}$$

while the initial ion density is such that

$$n_{i0} = \begin{cases} n_0 & \text{for} \quad 0 \leqslant x \leqslant L/2, \\ 0 & \text{for} \quad L/2 \leqslant x \leqslant A. \end{cases} \tag{4.10}$$

The initial potential ϕ_0 is obtained by solving the nonlinear Poisson equation (2.7) associated with the initial electron and ion densities (4.9) and (4.10) and with the boundary conditions (4.8). The distribution functions are initialized by

$$f_{e0} = n_{e0} M_e(v), \quad f_{i0}(x, v) = n_{i0} M_i(v), \tag{4.11}$$

where the electron and ion Maxwellians are given by

$$M_e(v) = (\varepsilon/(2\pi))^{1/2} \exp(-\varepsilon v^2/2), \quad M_i(v) = (2\pi\eta)^{-1/2} \exp(-v^2/(2\eta)), \tag{4.12}$$

and $\eta = T_{i0}/T_{e0}$ is the ion to electron temperature ratio. In this test problem, $\eta = 10^{-3}$, and $L/2 = 20\lambda$.

In [23], the numerical parameters are chosen as follows. The simulation domain length is $A = 3 \times 10^4 \lambda$. The space step is $\Delta x = 0.2\lambda$ and there are 4×10^5 particles per cell. This makes a total number of 6×10^{10} particles, which exceeds our own computer resources. For this reason, we use a smaller simulation domain $A = 10^3 \lambda$ with the same $\Delta x = 0.2\lambda$ and 2000 particles per cell (1000 electrons and 1000 ions), which amounts to about 5×10^6 particles in total.

4.4.2. Simulation 1: time and space resolved case (reference case)

We first use the same time-step as [23] i.e. $\Delta t = 0.05\omega^{-1}$, where $\omega = 1/(\sqrt{\varepsilon}\lambda)$ is the electron plasma frequency and we view the results at time $T = 30\omega_i^{-1}$ where $\omega_i = \sqrt{\varepsilon}\omega$ is the ion plasma frequency. These time and space steps obviously resolve the plasma period and Debye length.

The electric potential and electric field are shown in Fig. 14 and should be compared with Fig. 9(a) and (b) of [23]. We observe that the boundary of the ion slab is located at $\sim 140\lambda$ as in [23]. This shows that the AP method gives a correct account of ion-acoustic waves, since the expansion roughly takes place at the speed of this wave. This correct account is preserved in the under-resolved case as shown in Sections 4.4.3 and 4.4.4. This observation suggests that the AP discretization does not modify waves that are present in quasineutral conditions, such as ion-acoustic or Alfven waves, even in under-resolved conditions.

We note that the values reached by the two electric field peaks, close to the center of the foil ($E \sim 0.01 E_0$) and at the boundary of the ion slab ($E \sim 0.03 E_0$), measured in units of $E_0 = (n_0 k_B T/\varepsilon_0)^{1/2}$ are in very good agreement with [23]. The ion density distribution is shown in Fig. 15(left) and the electron velocity distribution, in Fig. 15(right). They must be

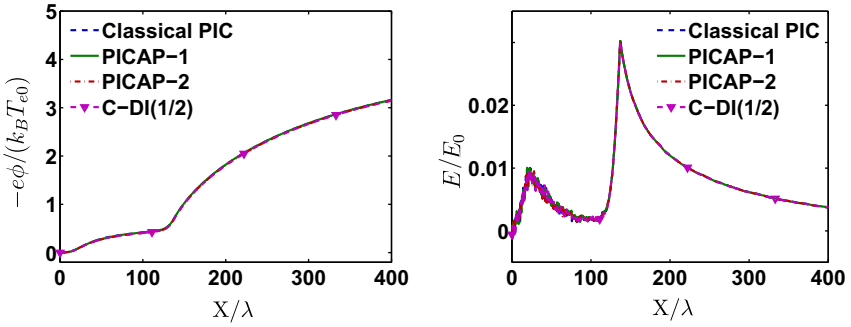

Fig. 14. Plasma expansion test case. Simulation 1: resolved case (reference case): $\Delta x = 0.2\lambda$ and $\Delta t = 0.05\ \omega^{-1}$. Electric potential (left) and electric field (right) as functions of position at time $t = 30\omega_i^{-1}$ with Classical PIC scheme, PICAP-1, PICAP-2 and Classical DI ($\beta = 1/2$) schemes. These pictures must be compared with Fig. 9(a) and (b) of Ref. [23].

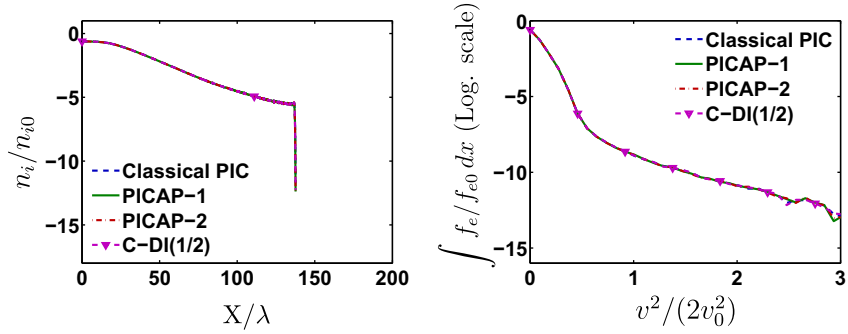

Fig. 15. Plasma expansion test case. Simulation 1: resolved case (reference case): $\Delta x = 0.2\lambda$ and $\Delta t = 0.05\ \omega^{-1}$. Ion density as a function of position in log scale (left) and electron velocity distribution as a function of $v^2/(2v_0^2)$ in log scale (right) with Classical PIC, PICAP-1, PICAP-2 and Classical DI ($\beta = 1/2$), at time $t = 30\omega_i^{-1}$. These pictures must be compared with Figs. 3(a) and 10 (respectively) of Ref. [23].

compared respectively with Fig. 10(a) and Fig. 3(a) of [23]. Note that we display the space-integrated velocity distribution function rather than the distribution function at $x = 0$ as in [23] because otherwise, there are too few particles to make a significant statistics. The ion and electron mean velocities are shown in Fig. 16 and should be compared with Fig. 10(b) of [23]. The ion density and velocity show an excellent agreement with [23]. The electron velocity distribution also shows similar features as in [23]: a flat top, then a steep gradient between 0.25 and 0.5 in units of $2v_0^2$ and then an abrupt change to a flatter gradient around 0.5. The electron mean velocities are quite noisy due to the lack of significant statistics in the region beyond the boundary of the ion slab. This large noise level is also apparent in [23].

4.4.3. Simulation 2: time and space under-resolved case

We now turn to fully under-resolved (in both time and space) simulations. To this aim, the space-step is set to the value $\Delta x = 4\lambda$, and the time-step, to the value $\Delta t = 3\omega^{-1}$. We present the electric potential and electric field in Fig. 18. We observe that the Classical PIC method gives nonsense: the order of magnitude of the potential and of the electric field have nothing to do with the true solution. The PICAP methods on the other hand give fairly good agreements with the reference solution. We still observe the same qualitative features as in the resolved case, with a peak electric field located at the boundary of the ion slab, and a smaller but distinct peak close to the center of the foil. On the other hand, the ion expansion is slowed down: the boundary of the ion slab is located at $x \sim 100\lambda$ in both PICAP-1 and PICAP-2 methods respectively as can be seen on the ion density profiles in Fig. 17(left). This reduction of the ion expansion can again be attributed to the lower precision of the method due to the large time and space steps (Δt is 60 times bigger than in the reference case, while Δx is $20t$ times bigger). All the Direct-Implicit schemes give less accurate results than the PICAP-1 and PICAP-2 schemes since they suffer from a lack of consistency in the quasi-neutral regime. The "best" Direct-Implicit schemes, the C-DI ($\beta = 1/2$) and the M-DI ($\beta = 1/2$), locate the boundary of the ion slab at $x \sim 75\lambda$, while the fully implicit M-DI ($\beta = 1$) locates this boundary at $x \sim 35\lambda$. We may expect an even better agreement of the PICAP schemes by the use of second order time discretizations. This point will be studied in future work.

Despite the slight degradation of accuracy, the PICAP methods provide fairly good results even in highly under-resolved situations, while the Classical PIC method fails completely, and the Direct-Implicit methods give poorer results. The use of much larger time and space steps leads to a considerable speed-up of the numerical simulation over fully-resolved PIC simulations which makes the PICAP methods attractive compromises between accuracy and computational efficiency.

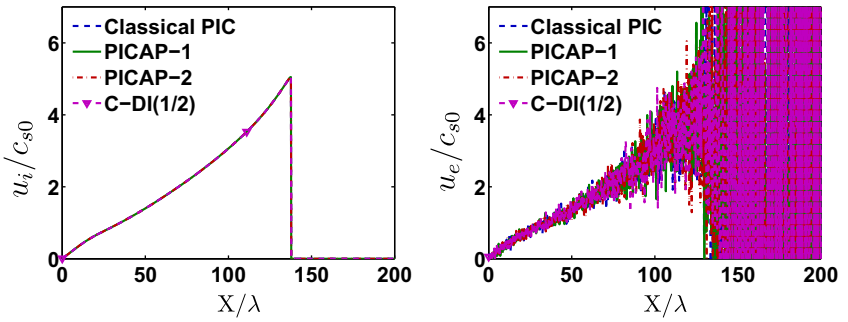

Fig. 16. Plasma expansion test case. Simulation 1: resolved case (reference case): $\Delta x = 0.2\lambda$ and $\Delta t = 0.05\ \omega^{-1}$. Ion and electron mean velocities as functions of position, with Classical PIC, PICAP-1, PICAP-2 and Classical DI ($\beta = 1/2$) schemes, at time $t = 30\omega_i^{-1}$ ($c_{s0} = \sqrt{k_B T_{e0}/m_i}$).

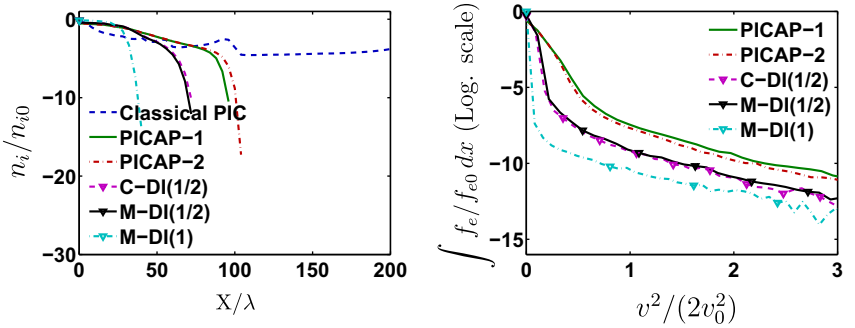

Fig. 17. Plasma expansion test case. Simulation 2: space and time under-resolved case: $\Delta x = 4\lambda$ and $\Delta t = 3\omega^{-1}$. Ion density as a function of position in log scale (left) and electron velocity distribution as a function of $v^2/(2v_0^2)$ in log scale (right) with Classical PIC, PICAP-1, PICAP-2, Classical DI ($\beta = 1/2$), Modified DI ($\beta = 1/2$) and Modified DI ($\beta = 1$) schemes, at time $t = 30\omega_i^{-1}$.

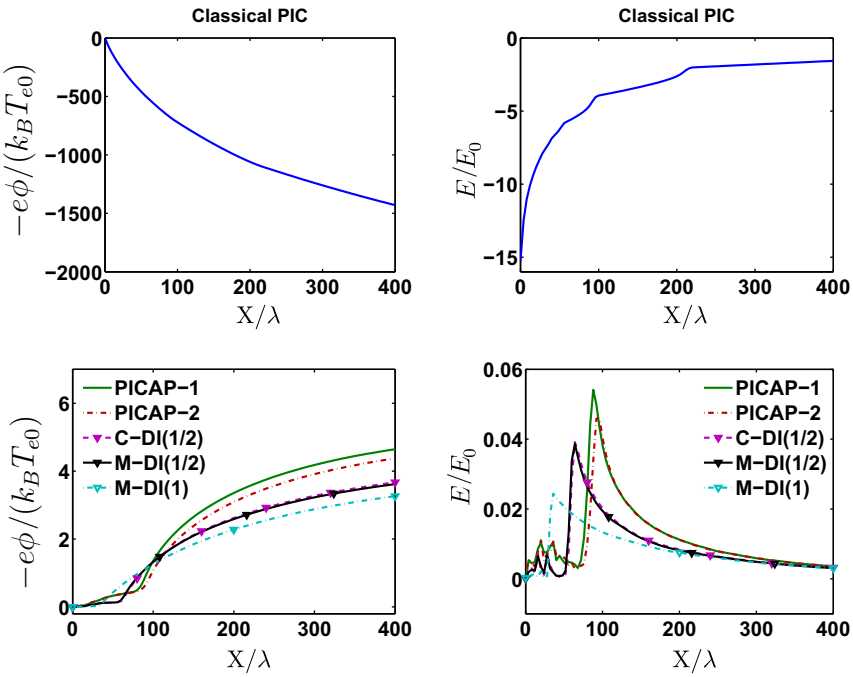

Fig. 18. Plasma expansion test case. Simulation 2: space and time under-resolved case: $\Delta x = 4\lambda$ and $\Delta t = 3\omega^{-1}$. Top: electric potential (left) and electric field (right) at time $t = 30\omega_i^{-1}$ as a function of position with classical PIC. Bottom: electric potential (left) and electric field (right) at time $t = 30\omega_i^{-1}$ as a function of position with PICAP-1, PICAP-2, Classical DI ($\beta = 1/2$), Modified DI ($\beta = 1/2$) and Modified DI ($\beta = 1$) schemes.

The ion density as a function of position (in log scale) and the electron velocity distribution as a function of $v^2/(2v_0^2)$ obtained in these under-resolved conditions are shown in Fig. 17(left and right respectively). Again, apart from the slower expansion of the slab, the ion density profiles given by the PICAP methods are quite good, with a sharp decrease at the boarder of the slab, while the Classical PIC method gives an almost uniform ion density, indicating that the ion slab has totally dissolved. We note that the PICAP-2 method seems slightly more accurate than the PICAP-1 method, as the ion expansion is faster with the former than with the latter. Both PICAP methods give more accurate results than the Direct-Implicit schemes. A close look at the electron velocity distribution shows that the PICAP methods better reproduce the distribution of low energy electrons ($v^2/2v_0^2 \leqslant 0.5$) than the Direct-Implicit methods, while the latter provide a better approximation of the large energy electrons ($v^2/2v_0^2 > 0.5$). It seems that a better account of the low energy electrons is preferable to provide a good description of the overall dynamics. The ion and electron mean velocities are shown in Fig. 19. With the PICAP methods, the general trend of the ion mean velocity is preserved. The maximal ion velocity (attained at the boundary of the ion slab) is smaller than in the reference case, which is again consistent with the slower expansion of the ion slab. With the Direct-Implicit methods, the ion velocity is scaled down further in accordance with the slower expansion velocity.

4.4.4. Simulation 3: time and space under-resolved with small number of particles

These simulations show that the PICAP methods are able to produce fairly accurate results at much lower cost than the Classical PIC method and with a better accuracy than the Direct-Implicit method. To emphasize this point, we now show simulation results using much less particles. Specifically, using the same under-resolved time and space steps, we now initialize the simulation with 1000 particles per mesh for each species, like in the reference simulation. Since the mesh size is 20 times bigger than in the reference simulation, there are 20 times less particles, namely a total of about 2.5×10^5 particles. The results are displayed in Figs. 20–22. The electric potential and electric field show almost no difference with the previous simulation using 20 times more particles (see Fig. 18). The boundary of the ion slab as appearing on the density profiles in Fig. 21(left), is located at the same position as in Fig. 17 (left). This indicates that the speed of the ion expansion is not affected by the number of particles. Because of the smaller number of particles, the statistics of the electron distribution function as appearing in Fig. 21(right) degrades at large velocities. However, for low velocities, the results are similar to the previous case (see Fig. 17(right)). The ion and electron mean velocities (Fig. 22) are also very similar to Fig. 19. The use of much larger time and space steps, together with a much smaller number of particles, results in considerably faster simulations. Of course, the price to pay is a slight degradation of accuracy. However, it appears that the PICAP method provides an interesting compromise between accuracy and computational efficiency and this accuracy is also sharper than the Direc-Implicit methods.

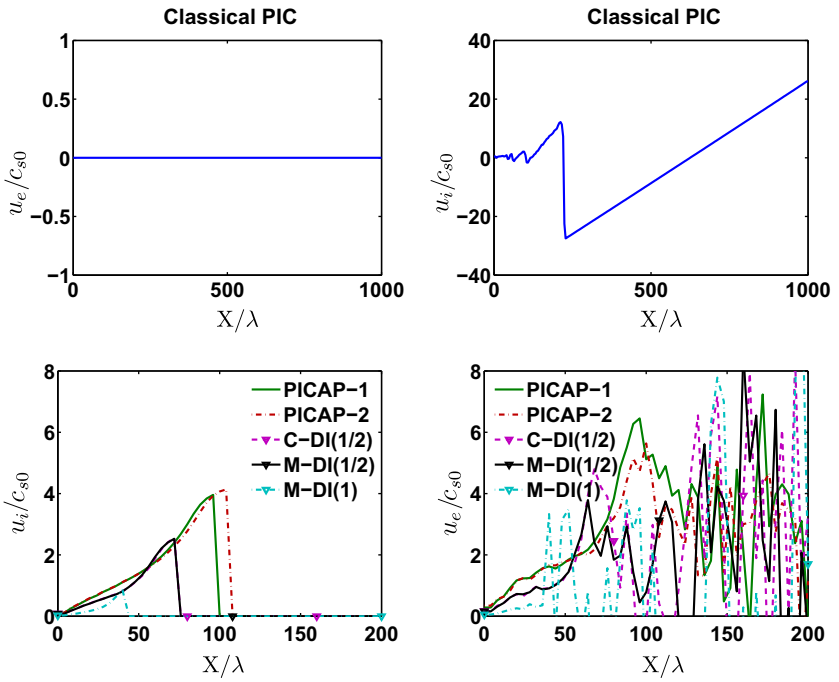

Fig. 19. Plasma expansion test case. Simulation 2: space and time under-resolved case: $\Delta x = 4\lambda$ and $\Delta t = 3\omega^{-1}$. Ion and electron mean velocities as functions of position, with Classical PIC (top), PICAP-1, PICAP-2, Classical DI ($\beta = 1/2$), Modified DI ($\beta = 1/2$) and Modified DI ($\beta = 1$) schemes (bottom), at time $t = 30\omega_i^{-1}(c_{s0} = \sqrt{k_B T_{e0}/m_i})$.

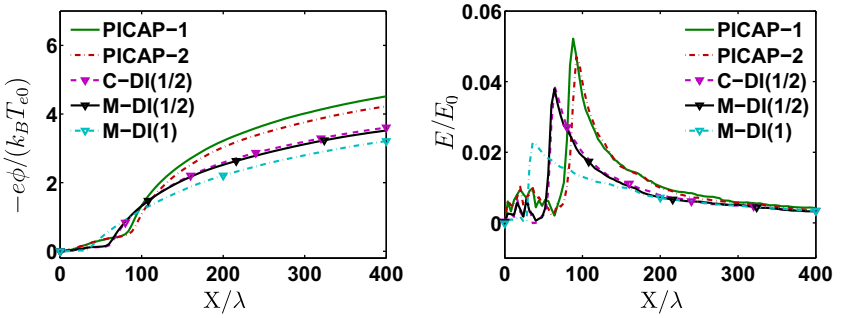

Fig. 20. Plasma expansion test case. Simulation 3: space and time under-resolved case: $\Delta x = 4\lambda$ and $\Delta t = 3\omega^{-1}$ and small number of particles (1000 particles per mesh and per species). Electric potential (left) and electric field (right) as a function of position with PICAP-1, PICAP-2, Classical DI ($\beta = 1/2$), Modified DI ($\beta = 1/2$) and Modified DI ($\beta = 1$) schemes at time $t = 30\omega_i^{-1}$.

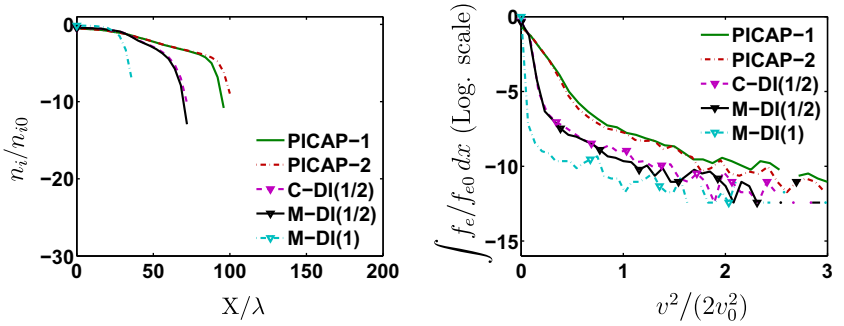

Fig. 21. Plasma expansion test case. Simulation 3: space and time under-resolved case: $\Delta x = 4\lambda$ and $\Delta t = 3\omega^{-1}$ and small number of particles (1000 particles per mesh and per species). Ion density as a function of position in log scale (left) and electron velocity distribution as a function of $v^2/(2v_0^2)$ in log scale (right) with Classical PIC, PICAP-1, PICAP-2, Classical DI ($\beta = 1/2$), Modified DI ($\beta = 1/2$) and Modified DI ($\beta = 1$) schemes, at time $t = 30\omega_i^{-1}$.

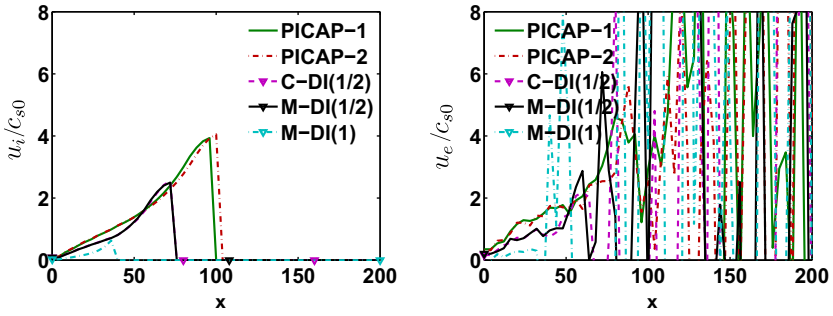

Fig. 22. Plasma expansion test case. Simulation 3: space and time under-resolved case: $\Delta x = 4\lambda$ and $\Delta t = 3\omega^{-1}$ and small number of particles (1000 particles per mesh and per species). Ion and electron mean velocities as functions of position, with PICAP-1, PICAP-2, Classical DI ($\beta = 1/2$), Modified DI ($\beta = 1/2$) and Modified DI ($\beta = 1$) schemes, at time $t = 30\omega_i^{-1}(c_{s0} = \sqrt{k_B T_{e0}/m_i})$.

Table 3
CPU speed-up per particle. Note that a smaller number of particles can be used in conjunction with the PICAP method, thereby increasing the CPU speed-up (see text).

	Simulation 1 Classical PIC fully resolved	Simulation 3 or 4 PICAP fully under-resolved	Speed-up per particle PICAP/ Classical PIC
CPU (s) per particle, per λ, per ω^{-1}	$2.88 \cdot 10^{-7}$	$6.0 \cdot 10^{-9}$	48

4.4.5. Computational speed-up and improvements

To illustrate this statement, we now compare the CPU time necessary to achieve the same final time-step, using the time and space resolved Classical PIC method on the one hand (Simulation 1), and the time and space under-resolved PICAP method on the other hand (Simulations 2 and 3). Table 3 displays the results. We normalize the CPU time to units of length and time equal to λ and ω^{-1} respectively and to one particle. Usually, the CPU time is normalized by the time and length steps but since the goal of the PICAP method is to use large time and space steps, we rather normalize the CPU time to the physical reference units.

The computational speed-up which can be obtained by the use of the PICAP method in the present situation is about 50 per particle. This means that Simulation 2, which uses the same number of particles as Simulation 1, is 50 times faster, but Simulation 3, which uses 20 times less particles, is about 1000 times faster. Given the extremely good qualitative agreement, this huge computationally speed-up can be extremely interesting for 2D and 3D simulations. Additionally, since the lower number of particles does not affect significantly the quality of the results, Simulation 3 also represents a considerable saving in terms of memory storage, which is also extremely interesting for higher dimensional simulations.

The degradation of accuracy related to the use of large time and space steps and small particle numbers seems to manifest itself in a slowing down of the time scales (such as that of the expansion of the ion slab). In general, in such circumstances, the method tends to overdamp the dynamics. However, the orders of magnitude are correct and the accuracy is significantly increased compared to Direct-Implicit methods. These tests also showed that there is no significant difference between the two PICAP methods, apart from a slightly lower dissipation by the PICAP-2 method. Additionally, the PICAP-2 method being a one-step time advancement method, it is easier to implement and should be preferred over PICAP-1.

In order to further increase the computational speed-up, one needs to bypass the limitation given by the CFL condition, namely that any given particle should not move more than one mesh size per time-step. We have tried to loosen the CFL condition, but this rapidly leads to unacceptable errors. The reason is that the PICAP method is not asymptotic preserving with respect to the particle masses. Since the electron mass is the smallest, the CFL constraint is more restrictive for the electrons. Therefore, it would be extremely useful to design an Asymptotic-Preserving PIC method associated with the small electron to ion mass ratio. Such a method is not available yet. A less efficient but probably easier method would be to use a local time-step and to take advantage of the less severe CFL constraint in the regions where the particle velocities are small. The use of a local space-step would also allow large cells in the regions of smooth gradients. In these regions, the CFL constraint could be locally loosened. Finally, the accuracy of the method could be increased by designing a second-order time integration method for the particle trajectories. All these research directions show that there exists a large potential of improvements for this method. These ideas will be implemented in future work.

5. Conclusion

In this paper, we have presented a novel PIC method for the Vlasov–Poisson equation. The method is Asymptotic Preserving in the quasineutral limit, i.e. it is consistent with the quasineutral Vlasov equation in the limit of vanishing

scaled Debye length. To validate this method, we have investigated several test problems: the first one consists of a steady state simulation; the second one considered a perturbation of a quasi neutral plasma with a particular consideration of the Landau damping; the third one is a bump-on-tail instability; the fourth one concerns the expansion of an ion slab in vacuum. All tests have confirmed that the method is stable even if the time and space steps are well above the values set by the plasma period and Debye length, while the standard PIC method is unstable in these conditions. The Direct-Implicit methods well capture plasma oscillations, but PICAP methods provide more consistent results for stiff test-cases such as the plasma expansion one. Despite the loss of accuracy associated with the use of large time and space steps, the method produces fairly accurate results and provides an attractive compromise between accuracy and computational efficiency. In the future, additional improvements of the method will be sought, such as for instance, removing the CFL constraint on the time-step or finding second-order accurate time discretizations of the particle trajectories. The method will also be extended to electromagnetic plasma simulations through the coupling of the Vlasov equations to the Maxwell equations.

Acknowledgments

This work has been supported by the Marie Curie Actions of the European Commission in the frame of the DEASE project (MEST-CT-2005-021122) and by the french "Commissariat à l'Energie Atomique (CEA)" in the frame of the contract ASTRE "SAV 34-180". It has been conducted while the fourth author was visiting the "Institut de Mathématiques de Toulouse" in the academic year 2007–2008 under the auspices of the China Scholarship Council. The authors wish to express their gratitude to J.C. Adam for helpful discussions and suggestions.

References

[1] T.D. Arber, R.G.L. Vann, A critical comparison of Eulerian-grid-based Vlasov solvers, J. Comput. Phys. 180 (2002) 339.
[2] R. Belaouar, N. Crouseilles, P. Degond, E. Sonnendrücker, An asymptotically stable semi-Lagrangian scheme in the quasi-neutral limit, J. Sci. Comput. 41 (2009) 341.
[3] C.K. Birdsall, A.B. Langdon, Plasma Physics via Computer Simulation, Taylor & Francis, 2004.
[4] J.U. Brackbill, D.W. Forslund, An implicit method for electromagnetic plasma simulation in two dimensions, J. Comput. Phys. 46 (1982) 271.
[5] Y. Brenier, Convergence of the Vlasov–Poisson system to the incompressible Euler equation, Comm. PDE 25 (2000) 737.
[6] J.A. Carrillo, F. Vecil, Nonoscillatory interpolation methods applied to Vlasov-based models, SIAM J. Sci. Comput. 29 (2007) 1179.
[7] F.F. Chen, Introduction to Plasma Physics and Controlled Fusion, Plenum Press, 1974.
[8] B.I. Cohen, A.B. Langdon, A. Friedman, Implicit time integration for plasma simulation, J. Comput. Phys. 46 (1982) 15.
[9] G.-H. Cottet, P.-A. Raviart, Particle methods for the one-dimensional Vlasov–Poisson equations, SIAM J. Numer. Anal. 21 (1984) 52.
[10] P. Crispel, P. Degond, M.-H. Vignal, An asymptotically stable discretization for the Euler–Poisson system in the quasineutral limit, C.R. Acad. Sci. Paris Ser. I 341 (2005) 323.
[11] P. Crispel, P. Degond, M.-H. Vignal, Quasi-neutral fluid models for current-carrying plasmas, J. Comput. Phys. 205 (2005) 408.
[12] P. Crispel, P. Degond, M.-H. Vignal, An asymptotic preserving scheme for the two-fluid Euler–Poisson model in the quasineutral limit, J. Comput. Phys. 223 (2007) 204.
[13] P. Degond, F. Deluzet, L. Navoret, An asymptotically stable particle-in-cell (PIC) scheme for collisionless plasma simulations near quasineutrality, C.R. Acad. Sci. Paris Ser. I 343 (2006) 613.
[14] P. Degond, J.G. Liu, M.-H. Vignal, Analysis of an asymptotic preserving scheme for the Euler–Poisson system in the quasineutral limit, SIAM Numer. Anal. 46 (2008) 1298.
[15] P. Degond, C. Parzani, M.-H. Vignal, Plasma expansion in vacuum: modeling the breakdown of quasineutrality, SIAM Multiscale Model. Simul. 2 (2003) 158.
[16] F. Filbet, E. Sonnendrcker, Comparison of Eulerian Vlasov solvers, Comput. Phys. Commun. 150 (2003) 247.
[17] A. Ghizzo, P. Bertrand, A Vlasov code for the numerical simulation of stimulated Raman scattering, J. Comput. Phys. 87 (1990) 495.
[18] A. Ghizzo, P. Bertrand, M. Shoucri, E. Fijalkow, M.R. Feix, An Eulerian code for the study of the drift-kinetic Vlasov equation, J. Comput. Phys. 108 (1993) 105.
[19] K. Ganguly, H.D. Victory Jr., On the convergence of particles methods for multidimensional Vlasov–Poisson systems, SIAM J. Numer. Anal. 26 (1989) 249.
[20] F. Golse, L. Saint-Raymond, The Vlasov–Poisson system with strong magnetic field in quasineutral regime, Math. Models Methods Appl. Sci. 13 (2003) 661.
[21] E. Grenier, Defect measures of the Vlasov–Poisson system in the quasineutral regime, Comm. P.D.E. 20 (1995) 1189.
[22] T. Grismayer, Etude thorique et numrique de l'expansion d'un plasma cr par laser: acclration d'ions haute nergie, Ph.D. dissertation, Ecole Polytechnique, Palaiseau, France, December 2006.
[23] T. Grismayer, P. Mora, J.C. Adam, A. Hron, Electron kinetic effects in plasma expansion and ion acceleration, Phys. Rev. E 77 (2008) 066407.
[24] S-Y. Ha, M. Slemrod, Global existence of plasma ion-sheaths and their dynamics, Comm. Math. Phys. 238 (2003) 149.
[25] D.W. Hewett, A.B. Langdon, Electromagnetic direct implicit plasma simulation, J. Comput. Phys. 72 (1987) 121.
[26] D.W. Hewett, C.W. Nielson, A multidimensional quasineutral plasma simulation model, J. Comput. Phys. 29 (1978) 219.
[27] R.W. Hockney, J.W. Eastwood, Computer Simulation Using Particles, Institute of Physics, 1988.
[28] S. Jin, Efficient asymptotic-preserving (AP) schemes for some multiscale kinetic equations, SIAM J. Sci. Comput. 21 (1999) 441.
[29] G. Joyce, M. Lampe, S.P. Slinker, W.M. Manheimer, Electrostatic particle-in-cell simulation technique for quasineutral plasma, J. Comput. Phys. 138 (1997) 540.
[30] N.A. Krall, A.W. Trivelpiece, Principles of Plasma Physics, San Francisco Press, 1986.
[31] A.B. Langdon, B.I. Cohen, A. Friedman, Direct implicit large time-step particle simulation of plasmas, J. Comput. Phys. 51 (1983) 107.
[32] A.B. Langdon, D.C. Barnes, Direct implicit plasma simulations, in: Multiple Time Scales, Academic Press, 1985.
[33] R.J. Mason, Implicit moment particle simulation of plasmas, J. Comput. Phys. 41 (1981) 233.
[34] R.J. Mason, Implicit moment PIC-hybrid simulation of collisional plasmas, J. Comput. Phys. 51 (1983) 484.
[35] R.J. Mason, Hybrid and collisional implicit plasma simulation models, in: Multiple Time Scales, Academic Press, 1985.
[36] R.J. Mason, An electromagnetic field algorithm for 2D implicit plasma simulation, J. Comput. Phys. 71 (1987) 429.
[37] Y.-J. Peng, Asymptotic limits of one-dimensional hydrodynamic models for plasma and semi-conductors, Chin. Ann. Math. B 23 (2002) 25.
[38] E. Pohn, M. Shoucri, G. Kamelander, Eulerian Vlasov codes, Comp. Phys. Commun. 166 (2005) 81.

[39] P.W. Rambo, Finite-grid instability in quasineutral hybrid simulations, J. Comput. Phys. 118 (1995) 152.
[40] F. Valentini, P. Trávincek, F. Califano, P. Hellinger, A. Mangeney, A hybrid-Vlasov model based on the current advance method for the simulation of collisionless magnetized plasma, J. Comput. Phys. 225 (2007) 753.
[41] J.M. Wallace, J.U. Brackbill, D.W. Forslund, An implicit moment electromagnetic plasma simulation in cylindrical coordinates, J. Comput. Phys. 63 (1986) 434.